

Article

# Robust Adaptive-Sliding-Mode Control for Teleoperation Systems with Time-Varying Delays and Uncertainties <sup>†</sup>

Yeong-Hwa Chang <sup>1,2,\*</sup> , Cheng-Yuan Yang <sup>1</sup> and Hung-Wei Lin <sup>1</sup><sup>1</sup> Department of Electrical Engineering, Chang Gung University, Taoyuan City 333, Taiwan<sup>2</sup> Department of Electrical Engineering, Ming Chi University of Technology, New Taipei City 243, Taiwan

\* Correspondence: yhchang@mail.cgu.edu.tw

<sup>†</sup> This paper is an extended version of our paper published in Y.-H. Chang, C.-Y. Yang and H.-W. Lin, “Adaptive control for bilateral teleoperation systems with time-varying delays”, 2018 IEEE International Conference on Applied System Invention (ICASI), Chiba, Japan, 2018, pp. 1111–1114, doi: 10.1109/ICASI.2018.8394475.

**Abstract:** Master–slave teleoperation systems with haptic feedback enable human operators to interact with objects or perform tasks in remote environments. This paper presents a sliding-mode control scheme tailored for bilateral teleoperation systems operating in the presence of unknown uncertainties and time-varying delays. To address unknown but bounded uncertainties, adaptive laws are derived alongside controller design. Additionally, a linear matrix inequality is solved to determine the allowable bound of delays. Stability of the closed-loop system is ensured through Lyapunov–Krasovskii functional analysis. Two-degree-of-freedom mechanisms are self-built as haptic devices. Free-motion and force-perception scenarios are examined, with experimental results validating and comparing performances. The proposed adaptive-sliding-control method increases the position performance from 58.48% to 82.55% and the force performance from 83.48% to 99.77%. The proposed control scheme demonstrates enhanced position tracking and force perception in bilateral teleoperation systems.

**Keywords:** adaptive control; sliding-mode control; teleoperation system; time-varying delays

**Citation:** Chang, Y.-H.; Yang, C.-Y.; Lin, H.-W. Robust Adaptive-Sliding-Mode Control for Teleoperation Systems with Time-Varying Delays and Uncertainties. *Robotics* **2024**, *13*, 89. <https://doi.org/10.3390/robotics13060089>

Academic Editor: Giovanni Muscato

Received: 21 April 2024

Revised: 30 May 2024

Accepted: 10 June 2024

Published: 13 June 2024



**Copyright:** © 2024 by the authors. Licensee MDPI, Basel, Switzerland. This article is an open access article distributed under the terms and conditions of the Creative Commons Attribution (CC BY) license (<https://creativecommons.org/licenses/by/4.0/>).

## 1. Introduction

The structure of teleoperation systems typically consists of several key components: human operator, master manipulator, slave manipulator, and communication channel. The interactions between these components form the basis of teleoperation systems, enabling human operators to control systems and interact with remote environments effectively [1,2]. In a teleoperation system, the human operator controls the master manipulator, usually through prescribed trajectories or specific tasks. The slave robot then follows the movements of the master manipulator in a free space, replicating the actions performed by the operator in the remote environment. Integrating haptic feedback into teleoperation systems enhances the operator’s situational awareness and dexterity, enabling more intuitive and precise control of the master manipulator while interacting with the remote environment. This contributes to improved task performance and overall efficiency in various teleoperation applications. The applications of teleoperation systems are versatile, such as in unmanned aerial vehicles [3–5], virtual reality [6,7], medical training [8–10], and telesurgery [11–16].

In recent years, significant advancements have been made in the development of teleoperation systems, with several methods and techniques being addressed to improve their performance, robustness, and versatility. In [17], an event-triggered mechanism combined with a PD-like controller was presented for bilateral teleoperation systems to address communication channel congestion. In [18], an adaptive proportional damping controller utilizing an RBF neural network and adaptive control strategy was proposed

to enhance stability and performance in a telerobotic system. On the other hand, time-domain-passivity control is a widely used approach to preserve the stability of teleoperation systems. In general, it is expected to maintain the passivity of the system to ensure a safe and stable operation [19,20]. Bavili et al. [21] investigated the problem of asymptotic stability and position tracking in nonlinear teleoperation systems when interacting with non-passive operators and environments. In [22], a passivity controller was presented to compensate for the non-passivity induced by longitudinal slipping and lateral sliding of wheeled robots. In [23], a passivity-based delay predictor was proposed to improve the transparency of a four-channel bilateral teleoperation system. Passivity-based control was utilized to ensure energy stability, and shared variable impedance control can facilitate smooth collaboration in teleoperation [24]. Additionally, a passivity-based nonlinear controller was introduced for bilateral teleoperation system under variable time delay and load disturbance [25]. In [26], a neural network-based four-channel-time-domain-passivity approach was proposed for a teleoperation system with time-varying delays.

Obtaining precise dynamic models for both master and slave manipulators in a teleoperation system can be challenging due to various factors such as nonlinearities, uncertainties, and complex mechanical structures. Adaptive tuning methods have been proposed to overcome this problem. Yang et al. [27] addressed the problem of adaptive tracking control for a teleoperation system with uncertainties in both kinematics and dynamics. In [28], an adaptive fuzzy neural network-backstepping-control scheme was developed for bilateral teleoperation systems to handle time delays and uncertainties. In [29], a fixed-time adaptive neural network-synchronization control was presented for teleoperation systems, handling position-error constraints and time-varying delays. In [30], a type-2 fuzzy neural network was proposed to deal with time-varying delays and uncertainties. In [31], a type-2 fuzzy-based observer was introduced to estimate external force/torque information and simultaneously filter out system disturbances. In [32], an adaptive bilateral control strategy was introduced for underwater manipulator teleoperation, with adaptive RBF network compensation for slave-manipulator uncertainties. In [33], a radial basis function-neural network-based-sliding-mode-control design was developed for nonlinear bilateral teleoperation system with transmission delays and uncertainties. In addition, a sliding-mode controller combined with a nonlinear-disturbance observer was proposed, such that the asymptotical stability can be preserved [34]. Due to the superiority of its robustness, the sliding-mode control has become an effective scheme for network control systems that are subject to time delays, packet losses, uncertainties, disturbances, and/or faults [35].

The presence of communication time delays and model uncertainties can significantly impact the transparency and stability of teleoperation systems [36,37]. For constant delays, a terminal sliding-mode controller was discussed for time-delayed nonlinear teleoperation systems [38]. In [39], an observer-based force control scheme was proposed to guarantee the position and force tracking in nonlinear teleoperation systems, subject to a constant communication time delay. Moreover, a bilateral neural network adaptive controller was designed for a class of teleoperation systems with constant time delays, external disturbances, and internal friction [40]. In practice, it is more attractive to investigate the tracking stability of teleoperation systems subject to time-varying delays. In [41], a general framework was presented to analyze and optimize the transparency of multilateral systems under time-varying delays. In [42], an adaptive control framework was developed to simultaneously handle both unknown kinematics/dynamics and time-varying delays. In [43], a finite-time control method was presented for bilateral teleoperators to ensure the coordination of master and slave manipulators in the presence of time-varying delays, external disturbances, and dynamic uncertainties. Zakerimanesh et al. [44] presented a control framework for bilateral teleoperation systems experiencing bounded time-varying delays in their communication channels.

When analyzing time-delay issues, delay-dependent approaches are generally less conservative than delay-independent approaches. However, the derivation of delay-dependent stability conditions can be more complex than that for delay-independent approaches, par-

ticularly because delays are explicitly considered in the design of stabilizing controllers. In general, when dealing with time-delay systems, ensuring closed-loop stability is crucial for the overall performance and reliability of the system. To achieve this, various conditions related to controller parameters are often desired, especially those that explicitly consider the time delays. Lyapunov–Krasovskii functions and linear matrix inequalities (LMIs) are commonly employed tools for investigating the stability of time-delay systems [45–51].

The synthesis problem in time-delayed teleoperation systems involves designing stabilizing controllers to ensure closed-loop stability while minimizing conservatism and preserving transparency in teleoperation. This entails finding less conservative stabilizing controllers that can effectively handle time delays, especially those that vary over time. Delay-dependent approaches are preferred due to their ability to explicitly consider time delays, which leads to more accurate estimation of stability conditions and efficient controller designs. By addressing practical considerations such as time-varying delays, teleoperation systems can achieve robust performance and seamless interaction between the operator and the remote environment. In the works of [52], both symmetric and asymmetric time-varying delays in communication were addressed. Symmetry of the communication delays means that the delays of the forward and backward channels are equal. Symmetric delays could exist in a constrained environment such as a local wire-connected network with a strictly defined protocol. On the other hand, asymmetric communication delays would be more practical in internet or wireless networks. In existing works of asymmetric time-varying delays, the bounds of time-varying delays are usually given in advance, then a delay-dependent controller can be obtained to ensure closed-loop stability. In this paper, it is desired to find the allowable boundary of time-varying communication delays. For the purpose of concise computations, a symmetric teleoperation system is addressed. How to relax this assumption of symmetry would be another interesting topic.

Transparency is a critical issue in teleoperations. Ensuring precise force feedback across versatile environments is a primary task. Our proposed control strategies are designed to maintain high transparency by accurately replicating forces encountered in the remote environment, thus enhancing the user’s sense of presence and control. In this work, a novel adaptive-sliding-mode control scheme is proposed for bilateral teleoperation systems encountering model uncertainties and time-varying delays. The main contributions are as follows:

1. The proposed method allows for the determination of admissible bounds of time-varying delays by solving linear matrix inequalities (LMIs), thus providing valuable insights into temporal constraints.
2. The derived adaptive laws enable the estimation of bounds for unknown uncertainties, thereby enhancing the robustness of the controller against model uncertainties.
3. Utilizing delay-dependent Lyapunov–Krasovskii functional analysis ensures the closed-loop stability of the teleoperation system, offering theoretical assurances even in the presence of delays and uncertainties.
4. The control scheme addresses both free-motion and force-perception aspects of a general non-passive teleoperation system, thereby expanding its applicability across various scenarios.
5. Conducting master–slave experiments validates the feasibility and effectiveness of the proposed control scheme in real-world settings, demonstrating its practical applicability and performance.

## 2. Materials and Methods

### 2.1. Preliminaries

The dynamic model for an  $n$ th degree master–slave robotic system can be described using the following equations:

$$M_m(q_m)\ddot{q}_m + C_m(q_m, \dot{q}_m)\dot{q}_m + g_m(q_m) + \delta_m = \tau_m + f_h \quad (1)$$

$$M_s(q_s)\ddot{q}_s + C_s(q_s, \dot{q}_s)\dot{q}_s + g_s(q_s) + \delta_s = \tau_s - f_e \tag{2}$$

where the subscripts  $m$  and  $s$  represent the master and slave, respectively,  $q_m$  and  $q_s \in \mathcal{R}^n$  are the vectors joint positions,  $M_m(q_m)$  and  $M_s(q_s) \in \mathcal{R}^{n \times n}$  are the inertia matrices,  $C_m(q_m, \dot{q}_m)$  and  $C_s(q_s, \dot{q}_s) \in \mathcal{R}^{n \times n}$  are the Coriolis matrices,  $g_m(q_m)$  and  $g_s(q_s) \in \mathcal{R}^n$  are the gravitational vectors,  $\tau_m$  and  $\tau_s \in \mathcal{R}^n$  are vectors of input torques,  $f_h$  and  $f_e \in \mathcal{R}^n$  are the human operation force and the environmental force, and  $\delta_m$  and  $\delta_s$  are the unknown uncertainties of the master and slave robots, respectively. In this paper, the human operator's force  $f_h$  and the environmental force  $f_e$  are non-passive [53,54]:

$$f_h = k_h - D_h \dot{q}_m - K_h q_m \tag{3}$$

$$f_e = k_e - D_e \dot{q}_s - K_e q_s \tag{4}$$

where  $k_h$  and  $k_e$  are constant vectors of  $\mathcal{R}^n$ , and  $D_h$  and  $K_h \in \mathcal{R}^{n \times n}$  are the damping and spring-constant matrices for human force, respectively. In addition,  $D_e$  and  $K_e \in \mathcal{R}^{n \times n}$  represent the damping and spring-constant matrices for the environmental force, respectively.

**Property 1.** The inertia matrix  $M_i(q_i)$  is symmetric and positive definite. Let  $\bar{\lambda}_i$  be the maximum eigenvalue of  $M_i(q_i)$ . Then,  $M_i(q_i) \leq \bar{\lambda}_i I_n$  where  $I_n \in \mathcal{R}^{n \times n}$  is the identity matrix,  $i \in \{m, s\}$ .

**Property 2.** The matrix  $\dot{M}_i(q_i) - 2C_i(q_i, \dot{q}_i)$  is skewed symmetric,  $i \in \{m, s\}$ .

**Property 3.** There exists a positive constant  $c_i$  such that  $\|C_i(q_i, \dot{q}_i)\|_2 \leq c_i$ , where  $\|\cdot\|_2$  represents the  $\mathcal{L}_2$  norm,  $i \in \{m, s\}$ .

**Assumption 1.** Let  $\delta_i = [\delta_{i1} \ \delta_{i2} \ \dots \ \delta_{in}]^T$  be bounded by  $\bar{\delta}_i = [\bar{\delta}_{i1} \ \bar{\delta}_{i2} \ \dots \ \bar{\delta}_{in}]^T$ ,  $|\delta_{ij}| < \bar{\delta}_{ij}$ , where  $\bar{\delta}_{ij}$  is an unknown constant,  $i \in \{m, s\}$ ,  $j = 1, 2, \dots, n$ .

**Lemma 1.** [55] Given a positive-definite matrix  $R$ , the following inequality holds

$$2X^T Y \leq X^T R X + Y^T R^{-1} Y, \tag{5}$$

where  $X$  and  $Y$  are two matrices with proper dimensions.

**Lemma 2.** [56] Let  $O = \begin{bmatrix} O_{11} & O_{12} \\ O_{12}^T & -O_{22} \end{bmatrix}$  be a matrix with proper dimensions,  $O_{22} > 0$ . Then the following equation holds:

$$O < 0 \iff O_{11} + O_{12} O_{22}^{-1} O_{12}^T < 0. \tag{6}$$

### 2.2. Adaptive-Sliding-Mode-Controller Design

In the context of the time-delayed teleoperation system described by Equations (1) and (2), a sliding-mode controller will be designed to achieve asymptotically stable sliding motion.

**Assumption 2.** The forward and backward communication delays are symmetric, and the time-varying delay  $d(t)$  satisfies the conditions that

$$0 < d(t) \leq \bar{d} < \infty, \dot{d}(t) \leq \mu < 1, \tag{7}$$

where  $\bar{d}$  and  $\mu$  are positive constants.

**Remark 1.** If  $\dot{d}(t) \geq 1$ , then the delay will grow faster than the increase in time. As the manipulator devices are required to track some delayed trajectories, the control loop becomes open. Under this circumstance, the controller design and related stability analysis opens a new theoretical problem, which cannot be solved at current stage and needs to be investigated separately [42].

In the following equations, the notations  $q_{m,d}$  and  $q_{s,d}$  are used to stand for  $q_m(t - d(t))$  and  $q_s(t - d(t))$ , respectively, for simplicity. The sliding surfaces for the master and slave robots are defined, respectively, as

$$\begin{aligned} s_m &= \dot{q}_m + K_m(q_m - q_{s,d}) \\ s_s &= \dot{q}_s + K_s(q_s - q_{m,d}) \end{aligned} \tag{8}$$

where  $K_m = \text{diag}\{k_{m1}, k_{m2}, \dots, k_{mn}\} \in \mathcal{R}^{n \times n}$  and  $K_s = \text{diag}\{k_{s1}, k_{s2}, \dots, k_{sn}\} \in \mathcal{R}^{n \times n}$ ,  $k_{mj} > 0$ , and  $k_{sj} > 0$ ,  $j = 1, 2, \dots, n$ . Then, the sliding mode of (8),  $s_m = s_s = 0$ , can be equivalently described as

$$\begin{aligned} \dot{q}_m &= -K_m(q_m - q_{s,d}) \\ \dot{q}_s &= -K_s(q_s - q_{m,d}) \end{aligned} \tag{9}$$

Let the error functions of the master and slave sides, respectively, be defined as

$$e_m = q_m - q_s, \quad e_s = q_s - q_m \tag{10}$$

From (9) and (10), it can be determined that

$$\dot{e} = -A_1 e - A_1 e_d \tag{11}$$

where  $e = [e_m^T \quad e_s^T]^T$ ,  $e_d = e(t - d(t))$ , and  $A_1 = \text{diag}\{K_m, K_s\}$ .

**Theorem 1.** *The error functions of (10) are asymptotically convergent if the following inequality holds:*

$$\begin{bmatrix} \Theta_{11} & A_1 P_s & \mathbf{0}_{2n} & A_1 \\ P_s A_1 & -\bar{d}^{-1} R_s & \mathbf{0}_{2n} & \mathbf{0}_{2n} \\ \mathbf{0}_{2n} & \mathbf{0}_{2n} & -\tilde{\mu} Q_s & A_1 \\ A_1 & \mathbf{0}_{2n} & A_1 & -(\bar{d} R_s)^{-1} \end{bmatrix} < 0 \tag{12}$$

where  $P_s$ ,  $Q_s$ , and  $R_s$  are symmetric positive-definite matrices of  $\mathcal{R}^{2n \times 2n}$ ,  $\Theta_{11} = -4P_s A_1 + Q_s$ ,  $\tilde{\mu} = 1 - \mu$ , and  $\mathbf{0}_{2n}$  is a zero matrix of dimension  $2n \times 2n$ .

**Proof.** A Lyapunov–Krasovskii function is chosen as

$$V_s = e^T P_s e + \int_{t-d(t)}^t e^T(s) Q_s e(s) ds + \int_{-\bar{d}}^0 \int_{t+\theta}^t \dot{e}^T(s) R_s \dot{e}(s) ds d\theta. \tag{13}$$

The time derivative of  $V_s$  from (11) is derived as

$$\begin{aligned} \dot{V}_s &\leq 2e^T P_s (-A_1 e - A_1 e_d) + e^T Q_s e - \tilde{\mu} e_d^T Q_s e_d \\ &\quad + \bar{d} (-A_1 e - A_1 e_d)^T R_s (-A_1 e - A_1 e_d) - \int_{t-\bar{d}}^t \dot{e}^T(s) R_s \dot{e}(s) ds \end{aligned} \tag{14}$$

It is noted that  $e_d = e - \int_{t-d(t)}^t \dot{e}(s) ds$ . Then, from Lemma 1 and Assumption 2, it leads to the following inequality

$$\begin{aligned} \dot{V}_s &\leq -4e^T P_s A_1 e + \bar{d} e^T P_s A_1 R_s^{-1} A_1 P_s e + e^T Q_s e - \tilde{\mu} e_d^T Q_s e_d + \bar{d} e^T A_1 R_s A_1 e \\ &\quad + 2\bar{d} e^T A_1 R_s A_1 e_d + \bar{d} e_d^T A_1 R_s A_1 e_d = \begin{bmatrix} e \\ e_d \end{bmatrix}^T \Theta \begin{bmatrix} e \\ e_d \end{bmatrix} \end{aligned} \tag{15}$$

where

$$\Theta = \begin{bmatrix} \Theta_1 & \bar{d}A_1R_sA_1 \\ \bar{d}A_1R_sA_1 & \bar{d}A_1R_sA_1 - \tilde{\mu}Q_s \end{bmatrix}, \Theta_1 = -4P_sA_1 + Q_s + \bar{d}P_sA_1R_s^{-1}A_1P_s + \bar{d}A_1R_sA_1 \quad (16)$$

From Lemma 2,  $\dot{V}_s$  is negative if (12) holds. This implies that the error dynamics of (11) is asymptotically stable. This completes the proof.  $\square$

The sliding-mode-based controllers for the torques acting on the delayed teleoperation system are designed as

$$\tau_m = \tau_{eq,m} + \tau_{sw,m} \quad (17)$$

$$\tau_s = \tau_{eq,s} + \tau_{sw,s} \quad (18)$$

where  $\tau_{eq,m}$  and  $\tau_{eq,s}$  are the equivalent control actions and  $\tau_{sw,m}$  and  $\tau_{sw,s}$  are the switching controllers. From (1) and (2), considering the uncertainty-free case, the equivalent controllers  $\tau_{eq,m}$  and  $\tau_{eq,s}$  can be determined as

$$\tau_{eq,m} = -M_mK_m(\dot{q}_m - \dot{q}_{s,d}) + C_m\dot{q}_m + g_m \quad (19)$$

$$\tau_{eq,s} = -M_sK_s(\dot{q}_s - \dot{q}_{m,d}) + C_s\dot{q}_s + g_s \quad (20)$$

It is noted that the uncertain terms  $\delta_m$  and  $\delta_s$  of (1) and (2) are unknown but bounded. To estimate  $\bar{\delta}_m = [\bar{\delta}_{m1} \ \bar{\delta}_{m2} \ \dots \ \bar{\delta}_{mn}]^T$  and  $\bar{\delta}_s = [\bar{\delta}_{s1} \ \bar{\delta}_{s2} \ \dots \ \bar{\delta}_{sn}]^T$ , the adaptive laws are designated as follows:

$$\dot{\hat{\delta}}_m = \begin{cases} \Gamma M_m^{-1}|s_m|, & \text{if } f_h = 0, \\ 0, & \text{if } f_h \neq 0. \end{cases} \quad (21)$$

$$\dot{\hat{\delta}}_s = \begin{cases} \Gamma M_s^{-1}|s_s|, & \text{if } f_e = 0, \\ 0, & \text{if } f_e \neq 0. \end{cases} \quad (22)$$

where  $\hat{\delta}_m$  and  $\hat{\delta}_s \in \mathcal{R}^n$ ,  $\Gamma = \text{diag}\{\gamma_1, \gamma_2, \dots, \gamma_n\} \in \mathcal{R}^{n \times n}$ ,  $\gamma_j > 0, j = 1, 2, \dots, n$ ,  $|s_m| = [|s_{m1}| \ |s_{m2}| \ \dots \ |s_{mn}|]^T$ , and  $|s_s| = [|s_{s1}| \ |s_{s2}| \ \dots \ |s_{sn}|]^T$ .

In this paper, the switching controllers are formulated as

$$\tau_{sw,m} = -(\Phi_m + \hat{\Delta}_m)\text{sgn}(s_m), \quad (23)$$

$$\tau_{sw,s} = -(\Phi_s + \hat{\Delta}_s)\text{sgn}(s_s), \quad (24)$$

in which  $\Phi_m = \text{diag}\{\phi_{m1}, \phi_{m2}, \dots, \phi_{mn}\} \in \mathcal{R}^{n \times n}$ ,  $\Phi_s = \text{diag}\{\phi_{s1}, \phi_{s2}, \dots, \phi_{sn}\} \in \mathcal{R}^{n \times n}$ ,  $\phi_{mj} > 0, \phi_{sj} > 0, j = 1, 2, \dots, n$ , and  $\text{sgn}(\cdot)$  is a standard sign function. In addition,  $\hat{\Delta}_m = \text{diag}\{\hat{\delta}_{m1}, \hat{\delta}_{m2}, \dots, \hat{\delta}_{mn}\}$  and  $\hat{\Delta}_s = \text{diag}\{\hat{\delta}_{s1}, \hat{\delta}_{s2}, \dots, \hat{\delta}_{sn}\}$ .

**Remark 2.** The required input torques on the master and slave sides are shown in (17) and (18). The input torques include both equivalent and switching control actions. For example, the input torque  $\tau_m$  can be obtained from  $\tau_{eq,m}$  and  $\tau_{sw,m}$  in Equations (17), (19) and (23). In (23), an adaptive law for the unknown bounded uncertainties is designed as (21). Similarly, the input torque  $\tau_s$  can be implemented with Equations (18), (20), (22), and (24). The scheme diagram of the proposed teleoperation system is shown in Figure 1.

**Remark 3.** There could be a potential issue of chattering associated with the use of the sign function in the controller (23) and (24). To address this common chattering problem, a smoothing technique can be employed by replacing the sign function with a continuous approximation, such as a saturation function or a boundary-layer approach.

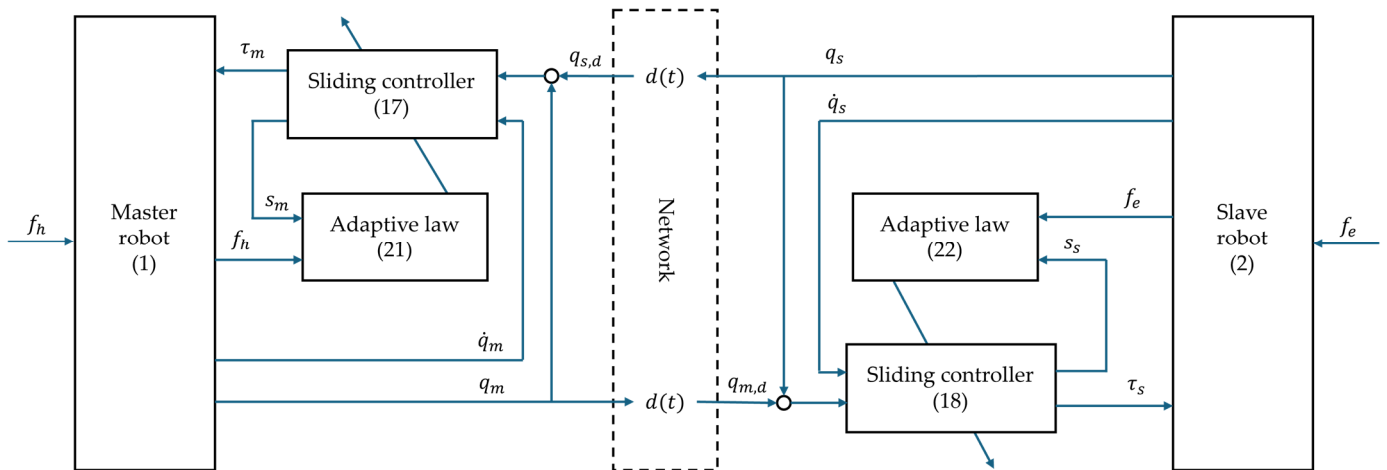


Figure 1. Adaptive-sliding-mode scheme for teleoperation system.

**Theorem 2.** Consider the bilateral teleoperation systems (1) and (2). In free motion,  $f_h = f_e = \mathbf{0}$ , and the state trajectories of teleoperation systems (1) and (2) will be driven onto the sliding surfaces (8) with the controllers (17) and (18) and the adaptive laws (21), (22).

**Proof.** Let a Lyapunov function be chosen as

$$V_c = \frac{1}{2} \left( s_m^T s_m + \tilde{\delta}_m^T \Gamma^{-1} \tilde{\delta}_m + s_s^T s_s + \tilde{\delta}_s^T \Gamma^{-1} \tilde{\delta}_s \right) \quad (25)$$

where  $\tilde{\delta}_m = \bar{\delta}_m - \hat{\delta}_m$ , and  $\tilde{\delta}_s = \bar{\delta}_s - \hat{\delta}_s$  are the estimation errors. The derivative of (8) is obtained as

$$\begin{aligned} \dot{s}_m &= \ddot{q}_m + K_m (\dot{q}_m - \dot{q}_{s,d}), \\ \dot{s}_s &= \ddot{q}_s + K_s (\dot{q}_s - \dot{q}_{m,d}). \end{aligned} \quad (26)$$

The derivative of  $V_c$  along (26) is

$$\begin{aligned} \dot{V}_c &= s_m^T \left( M_m^{-1} (\tau_m - C_m \dot{q}_m - g_m - \delta_m) + K_m (\dot{q}_m - \dot{q}_{s,d}) \right) \\ &+ s_s^T \left( M_s^{-1} (\tau_s - C_s \dot{q}_s - g_s - \delta_s) + K_s (\dot{q}_s - \dot{q}_{m,d}) \right) - \tilde{\delta}_m^T \Gamma^{-1} \dot{\tilde{\delta}}_m - \tilde{\delta}_s^T \Gamma^{-1} \dot{\tilde{\delta}}_s. \end{aligned} \quad (27)$$

From Assumption 1, this gives the following:

$$\begin{aligned} \dot{V}_c &< s_m^T \left( M_m^{-1} (\tau_m - C_m \dot{q}_m - g_m) + K_m (\dot{q}_m - \dot{q}_{s,d}) \right) \\ &+ s_s^T \left( M_s^{-1} (\tau_s - C_s \dot{q}_s - g_s) + K_s (\dot{q}_s - \dot{q}_{m,d}) \right) \\ &+ |s_m|^T M_m^{-1} \bar{\delta}_m + |s_s|^T M_s^{-1} \bar{\delta}_s - \tilde{\delta}_m^T \Gamma^{-1} \dot{\tilde{\delta}}_m - \tilde{\delta}_s^T \Gamma^{-1} \dot{\tilde{\delta}}_s. \end{aligned} \quad (28)$$

Substituting (17), (18), and (21) into (28), it yields

$$\dot{V}_c < -s_m^T \Phi_m M_m^{-1} \text{sgn}(s_m) - s_s^T \Phi_s M_s^{-1} \text{sgn}(s_s) \quad (29)$$

From (25) to (29), it is evident that the negative definiteness of  $V_c$  can be preserved, which means that  $s_m$ ,  $s_s$ ,  $\tilde{\delta}_m$ , and  $\tilde{\delta}_s$  are bounded. Therefore, the systems (1) and (2) are stable. Hence, the states of the teleoperation system (1) and (2) will reach the sliding surface (8). The proof is completed.  $\square$

### 2.3. Stability Analysis

Substituting (3), (4), (17), and (18) into (1) and (2), the closed-loop teleoperation systems can be represented as

$$\begin{aligned} M_m \ddot{q}_m &= -M_m K_m (\dot{q}_m - \dot{q}_{s,d}) + \epsilon_m + k_h - D_h \dot{q}_m - K_h q_m \\ M_s \ddot{q}_s &= -M_s K_s (\dot{q}_s - \dot{q}_{m,d}) + \epsilon_s + k_e - D_e \dot{q}_s - K_e q_s. \end{aligned} \tag{30}$$

where  $\epsilon_m = -\delta_m - \hat{\Delta}_m \text{sgn}(s_m) - \Phi_m \text{sgn}(s_m)$  and  $\epsilon_s = -\delta_s - \hat{\Delta}_s \text{sgn}(s_s) - \Phi_s \text{sgn}(s_s)$ .

**Remark 4.** According to Assumption 1 and Theorem 2, the uncertainty terms  $\delta_m$  and  $\delta_s$  are bounded and the estimated terms  $\hat{\Delta}_m$  and  $\hat{\Delta}_s$  are bounded. Thus, both the  $\epsilon_m$  and  $\epsilon_s$  are bounded.

**Theorem 3.** With non-passive human and environment forces (3) and (4), the closed-loop teleoperation system (30) is asymptotic stable if the following LMI holds:

$$\Omega = \begin{bmatrix} \Omega_{11} & \mathbf{0}_n & \mathbf{0}_n & \mathbf{0}_n \\ \mathbf{0}_n & \bar{\lambda}_s K_s - \tilde{\mu} Q & \mathbf{0}_n & \mathbf{0}_n \\ \mathbf{0}_n & \mathbf{0}_n & \Omega_{33} & \mathbf{0}_n \\ \mathbf{0}_n & \mathbf{0}_n & \mathbf{0}_n & \bar{\lambda}_m K_m - \tilde{\mu} Q \end{bmatrix} < \mathbf{0} \tag{31}$$

where  $Q \in \mathcal{R}^{n \times n}$  is a symmetric positive-definite matrix, and

$$\begin{aligned} \Omega_{11} &= -\bar{\lambda}_m K_m + (2c_m + \alpha_m) I_n + Q - 2D_h \\ \Omega_{33} &= -\bar{\lambda}_s K_s + (2c_s + \alpha_s) I_n + Q - 2D_e \end{aligned} \tag{32}$$

in which  $\alpha_m$  and  $\alpha_s$  are positive constants and  $0_n$  is a zero matrix of  $\mathcal{R}^{n \times n}$ .

**Proof.** Consider a Lyapunov–Krasovskii function candidate as follows:

$$\begin{aligned} V &= \dot{q}_m^T M_m \dot{q}_m + q_m^T K_h q_m + \int_{t-d(t)}^t \dot{q}_m^T(s) Q \dot{q}_m(s) ds + \dot{q}_s^T M_s \dot{q}_s \\ &\quad + q_s^T M_s q_s + \int_{t-d(t)}^t \dot{q}_s^T(s) Q \dot{q}_s(s) ds \end{aligned} \tag{33}$$

From Property 2, the time derivative of  $V$  along (30) can be reformulated as

$$\begin{aligned} \dot{V} &\leq 2\dot{q}_m^T \left( -M_m K_m (\dot{q}_m - \dot{q}_{s,d}) + C_m \dot{q}_m + \epsilon_m + k_h - D_h \dot{q}_m \right) \\ &\quad + 2\dot{q}_s^T \left( -M_s K_s (\dot{q}_s - \dot{q}_{m,d}) + C_s \dot{q}_s + \epsilon_s + k_e - D_e \dot{q}_s \right) \\ &\quad + \dot{q}_m^T Q \dot{q}_m - \tilde{\mu} \dot{q}_{m,d}^T Q \dot{q}_{m,d} + \dot{q}_s^T Q \dot{q}_s - \tilde{\mu} \dot{q}_{s,d}^T Q \dot{q}_{s,d}. \end{aligned} \tag{34}$$

From Lemma 1, the following inequalities can be obtained:

$$\begin{aligned} 2\dot{q}_m^T (\epsilon_m + k_h) &\leq \alpha_m \dot{q}_m^T \dot{q}_m + \frac{1}{\alpha_m} \|\epsilon_m + k_h\|_2^2 \\ 2\dot{q}_s^T (\epsilon_s + k_e) &\leq \alpha_s \dot{q}_s^T \dot{q}_s + \frac{1}{\alpha_s} \|\epsilon_s + k_e\|_2^2 \end{aligned} \tag{35}$$

and

$$\begin{aligned} 2\dot{q}_m^T K_m M_m \dot{q}_{s,d} &\leq \dot{q}_m^T K_m M_m \dot{q}_m + \dot{q}_{s,d}^T K_m M_m \dot{q}_{s,d} \\ 2\dot{q}_s^T K_s M_s \dot{q}_{m,d} &\leq \dot{q}_s^T K_s M_s \dot{q}_s + \dot{q}_{m,d}^T K_s M_s \dot{q}_{m,d} \end{aligned} \tag{36}$$

where  $\|\cdot\|_2$  represents the  $L_2$  norm of the signals.

From Properties 1 and 3, substituting (35) and (36) into (34) yields

$$\dot{V} \leq \dot{q}^T \Omega \dot{q} + \frac{1}{\alpha_m} \|\epsilon_m + k_h\|_2^2 + \frac{1}{\alpha_s} \|\epsilon_s - k_e\|_2^2 \tag{37}$$

where  $\dot{q} = [\dot{q}_m^T \quad \dot{q}_{m,d}^T \quad \dot{q}_s^T \quad \dot{q}_{s,d}^T]^T$ . Furthermore, it leads to the following condition,

$$V \leq \bar{\lambda}_\Omega \|\dot{q}\|_2^2 + \rho \tag{38}$$

where  $\bar{\lambda}_\Omega < 0$  is the maximum eigenvalue of the matrix  $\Omega$ ,  $\rho = \frac{1}{\alpha_m} \|\epsilon_m + k_h\|_2^2 + \frac{1}{\alpha_s} \|\epsilon_s - k_e\|_2^2$ . Noting that  $\rho$  is bounded,  $\rho \leq \bar{\rho}$ ,  $\bar{\rho}$  is a constant. Hence,  $\dot{V}$  is negative, if  $\|\dot{q}\|_2 > \sqrt{\frac{\bar{\rho}}{-\bar{\lambda}_\Omega}}$ . The controller parameters  $K_m$  and  $K_s$  can be chosen such that  $\dot{q}$  will be arbitrarily small. Therefore, the closed-loop system (30) is asymptotically stable.  $\square$

### 3. Experimental Results

In this paper, the master and slave devices are a pair of two-degrees-of-freedom-revolute-prismatic robots. The configuration illustration and 3D framework of the teleoperation devices are shown in Figure 2.

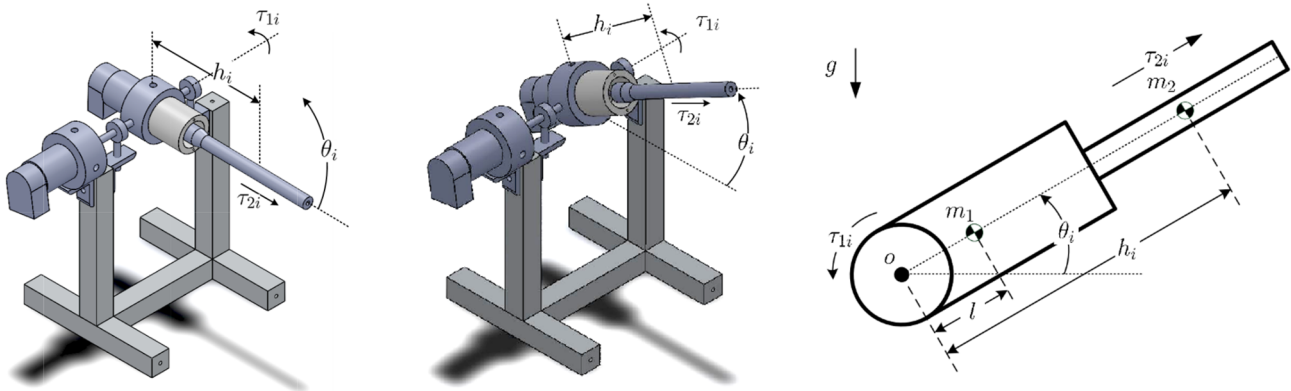


**Figure 2.** Configuration diagram of the master- and slave-manipulator robots.

The system parameters of the master and slave robots are listed in Table 1.

**Table 1.** System parameters of teleoperation systems.

$m_1$	Mass of link 1	0.36 kg
$m_2$	Mass of link 2	0.027 kg
$l$	Distance between joint o and center of link 1	0.02 m
$g$	Gravitational constant	9.8 m/s <sup>2</sup>

The dynamic models of (1) and (2) are obtained as

$$M_i(q_i) = \begin{bmatrix} m_1 l^2 + m_2 h_i^2 & 0 \\ 0 & m_2 \end{bmatrix}, C_i(q_i, \dot{q}_i) = \begin{bmatrix} 0 & 2m_2 h_i \dot{\theta}_i \\ -m_2 h_i \dot{\theta}_i & 0 \end{bmatrix}, \tag{39}$$

$$G_i(q_i) = \begin{bmatrix} (m_1 l + m_2 h_i) g \cos(\theta_i) \\ m_2 g \sin(\theta_i) \end{bmatrix}$$

$q_i = [\theta_i \ h_i]^T$ ,  $\dot{q}_i = [\dot{\theta}_i \ \dot{h}_i]^T$ ,  $\tau_i = [\tau_{1i} \ \tau_{2i}]^T$ ,  $f_h = [f_{h1} \ f_{h2}]^T$ ,  $f_e = [f_{e1} \ f_{e2}]^T$ ,  $i \in \{m, s\}$ . In addition,  $h_i$  is the length of the joint 2 between the point o and the center of mass of the second link, and  $\theta_i$  is the angle of the joint 1.

The parameters of the adaptive-sliding-mode controller are set as  $K_i = \text{diag}\{2, 2\}$ ,  $\Phi_i = \text{diag}\{2.5, 2.5\}$ , and  $\Gamma = \text{diag}\{0.5, 0.1\} \times 10^{-3}$ ,  $i \in \{m, s\}$ . The disturbance parts are assumed as  $\delta_i = \text{diag}\{0.5, 0.1\} \times \text{rand}(\cdot) \times 10^{-3}$  and  $\text{rand}(\cdot)$  is a uniformly distributed random number. From Theorem 1, the allowable delay bound can be obtained as  $\bar{d} = 0.5$  s by solving LMI (12). In experiments, the time delay is chosen as  $d(t) = 0.25 + 0.2\sin(t)$  s. The initial states of the master and slave robots are set as  $q_m = q_s = [0 \ 0.145]^T$ , and the initial velocities and acceleration are zero. Three types of controllers are adopted for comparison, including the proportional plus damping controller (P + dC) [17,18,45], sliding-mode controller (SC), and the proposed adaptive-sliding-mode controller (ASC). The following indices are considered for performance comparisons: the integral absolute error (IAE), the integral time absolute error (ITAE), the integral square error (ISE), and the integral time square error (ITSE) [57].

In the following, the cases of both free motion and force perception are performed. The experimental setup of a bilateral teleoperation system is shown in Figure 3. The position responses of the master and slave robots are measured by encoders. The control algorithms and signal interfacing are implemented by Raspberry Pi and a PIC18F4331 microprocessor. The sampling time is selected as 20 ms. In these experiments, the time delay is realized by software programming. Furthermore, all of the controller parameters of the teleoperation system are the same as the settings in simulations. The allowable delay bound is determined to be 0.5 s. The behavior of a delay can be accurately captured if the delay is multiple times the length of the sampling time.

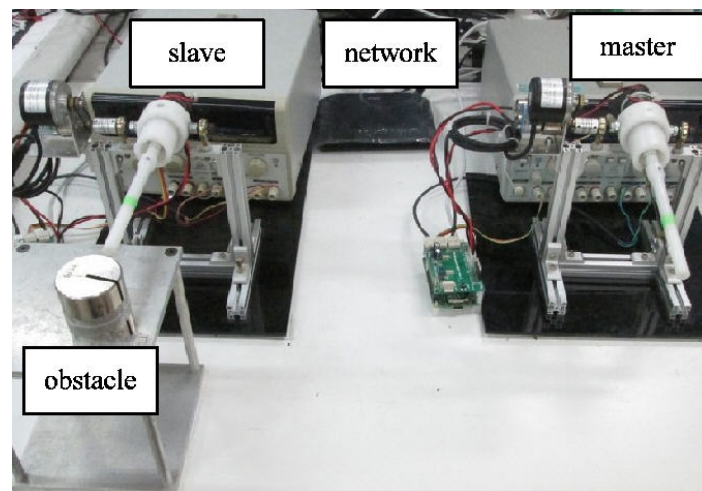
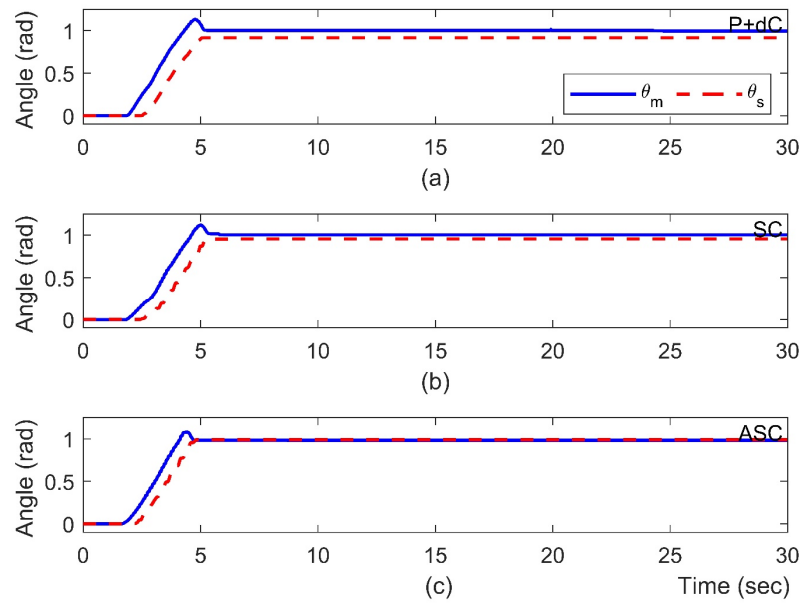


Figure 3. Experimental setup for teleoperation system.

### 3.1. Case 1: Free Motion (Experiment)

During the free-motion operation, the human operator moves the master robot towards  $\theta_m = 1$  rad and  $h_m = 0.195$  m, and the operator leaves the device standing still alone for  $t > 5$  s. It is desired to see whether the slave robot can track the motion trajectory of the master device stably. As shown in Figures 4 and 5, the steady-state position errors are significantly reduced using the ASC method. Quantitative analyses of different methods are shown in Table 2. The proposed ASC method increases the performance improvement from 70.70% to 90.00%. The video snapshots captured from the ASC are depicted in Figure 6, where the recording time of each snapshot is indicated on the bottom right.



**Figure 4.** Position responses of joint 1 with different control methods for Case 1: (a) P + dC, (b) SC, and (c) ASC.

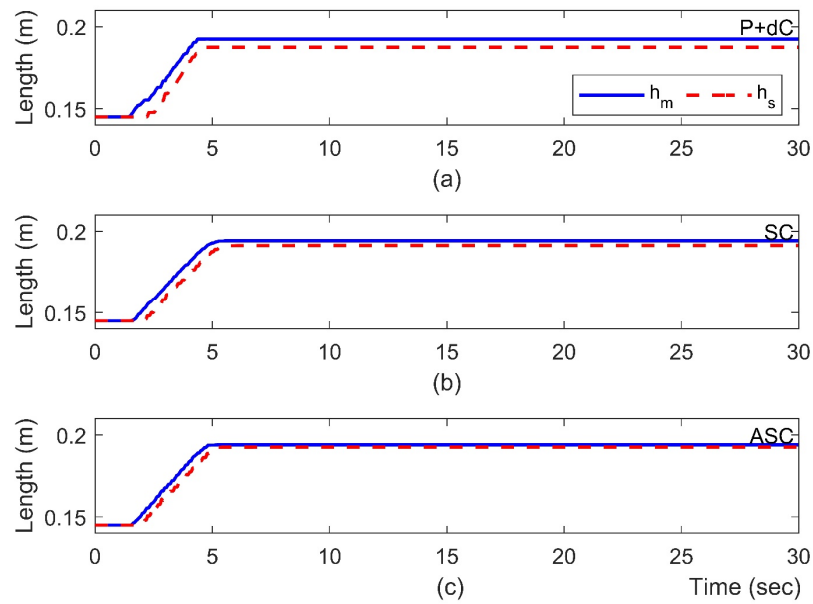


**Figure 5.** Position responses of joint 2 with different control methods for Case 1: (a) P + dC, (b) SC, and (c) ASC.

**Table 2.** Experimental comparisons of position errors in Case 1.

		IAE	ITAE	ISE	ITSE
P + dC	Joint 1	21.38	147.72	1983.70	199.68
	Joint 2	0.045	7.79	115.41	0.60
SC	Joint 1	13.38	99.21	1199.80	92.06
	Joint 2	0.019	4.81	68.24	0.21
ASC	Joint 1	6.26	36.91	248.95	22.71
	Joint 2	0.008	2.70	33.85	0.06

unit: joint 1 (rad), joint 2 (m).

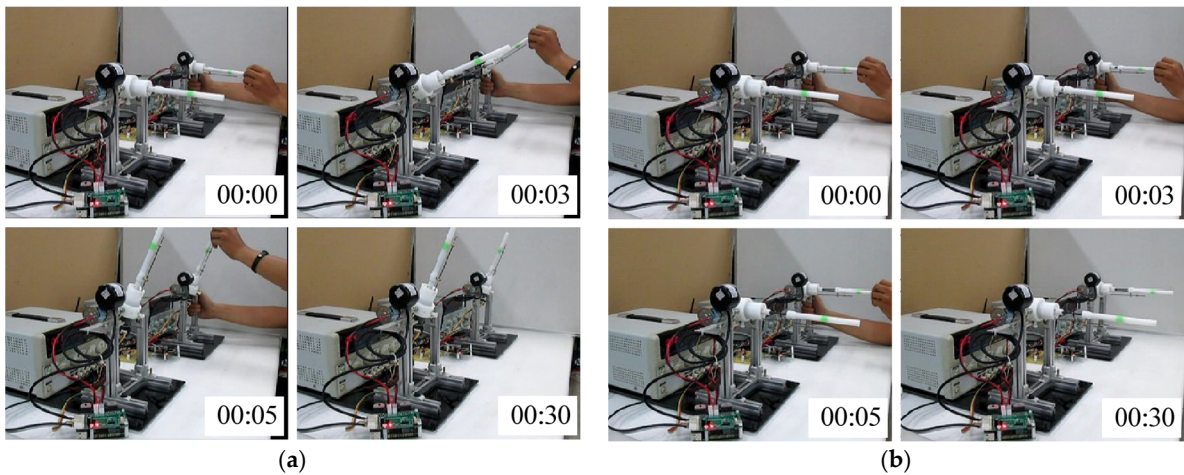


**Figure 6.** The snapshots of the experimental results for Case 1 (ASC): (a) joint 1, and (b) joint 2.

3.2. Case 2: Force Perception (Experiment)

In this case, an obstacle is placed on the slave side of the system at a position of roughly  $h_s = 0.175$  m and  $\theta_s = -0.5$  rad, respectively. As it is following the scheduled movement of the master, the slave robot will contact the pre-placed obstacle. Like in the simulation discussions, the force feedback will be conducted in turn for each joint. The experimental results corresponding to different methods are presented in Figures 7–10, where the slave robot contacts the obstacle around  $t = 4$  s. From Figures 7 and 8, it can be observed that there exist quite clear biases between the joint positions of master and slave robots with the P + dC method. On the other hand, the proposed ASC controller can provide significant improvements in position tracking and force perception. As the force perception in Figures 9 and 10, the proposed ASC control method has superiority in stably and accurately tracking for  $t > 4$  s. Quantitative analyses of the experimental results are summarized in Tables 3 and 4. They indicate that the proposed ASC method increases position performance from 58.48% to 82.55% and improves force performance from 83.48% to 99.77%. The video snapshots of ASC are depicted in Figure 11, where the recording time of each snapshot is indicated on the bottom right.

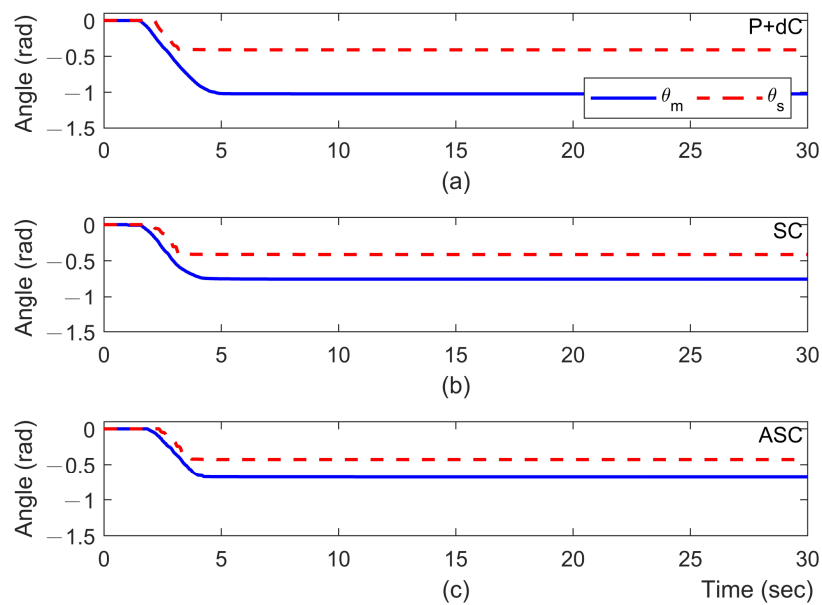


**Figure 7.** Position responses of joint 1 with different control methods for Case 2: (a) P + dC, (b) SC, and (c) ASC.

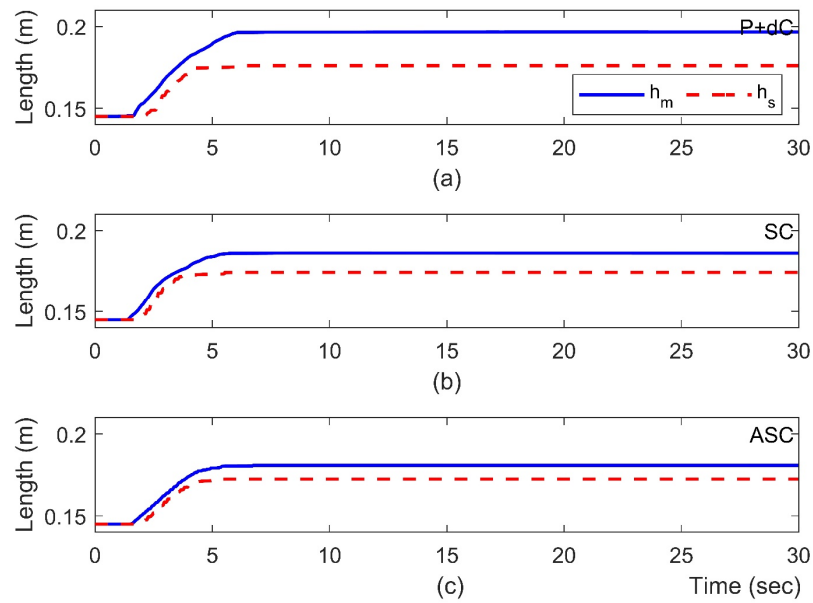


**Figure 8.** Position responses of joint 2 with different control methods for Case 2: (a) P + dC, (b) SC, and (c) ASC.

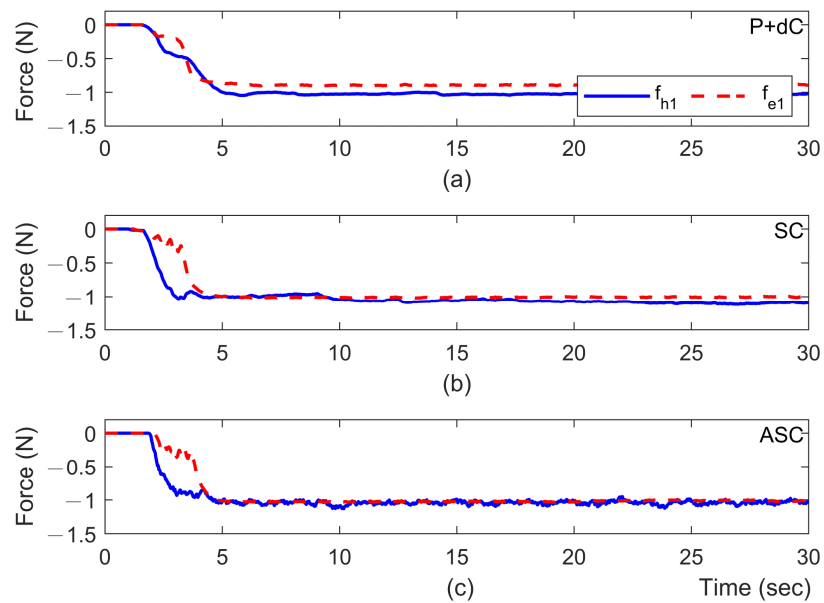


**Figure 9.** Force responses of joint 1 with different control methods for Case 2: (a) P + dC, (b) SC, and (c) ASC.

**Table 3.** Experimental comparisons of position responses in Case 2.

		IAE	ITAE	ISE	ITSE
P + dC	Joint 1	493.82	822.78	13,620.00	8319.10
	Joint 2	0.53	27.06	453.25	9.23
SC	Joint 1	155.35	465.18	7588.70	2575.70
	Joint 2	0.18	15.84	262.65	3.09
ASC	Joint 1	85.66	343.22	5655.00	1432.80
	Joint 2	0.17	15.69	241.20	2.60

unit: joint 1 (rad), joint 2 (m).

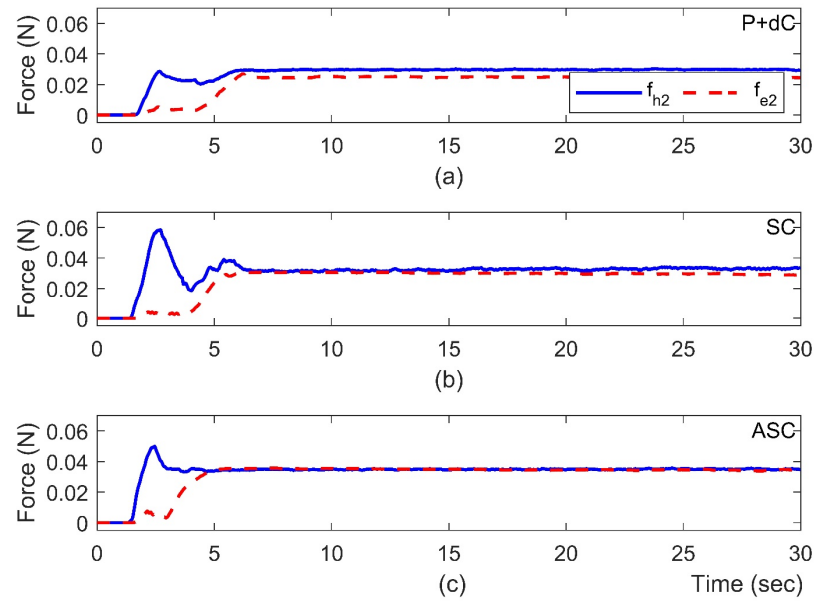


**Figure 10.** Force responses of joint 2 with different control methods for Case 2: (a) P + dC, (b) SC, and (c) ASC.

**Table 4.** Experimental comparisons of force errors in Case 2.

		IAE	ITAE	ISE	ITSE
P + dC	Joint 1	24.45	178.45	2497.80	351.22
	Joint 2	0.048	7.23	85.57	0.435
SC	Joint 1	13.28	93.91	1348.60	112.79
	Joint 2	0.036	4.77	54.07	0.195
ASC	Joint 1	2.87	34.35	412.59	15.84
	Joint 2	0.001	0.93	10.41	0.001

unit: joint 1 (N), joint 2 (N).

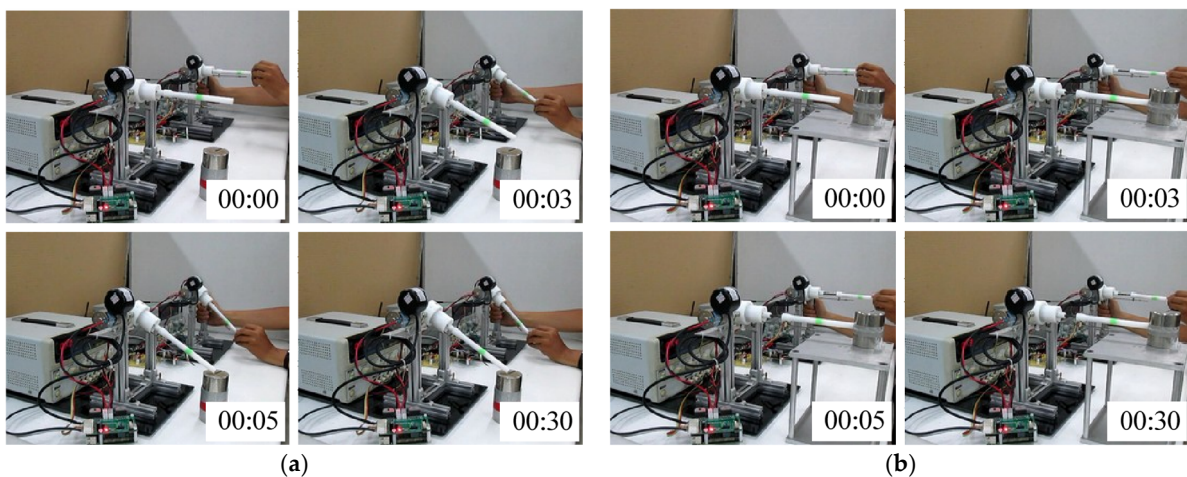


**Figure 11.** Snapshots of the experimental results for Case 2 (ASC): (a) joint 1, and (b) joint 2.

**Remark 5.** To enhance the reader's understanding of the experimental process and results, experimental videos have been uploaded to YouTube (accessed on 11 June 2024).

<https://www.youtube.com/watch?v=M0uSr1mg5YU>

[https://www.youtube.com/watch?v=buR8rsf2\\_ls](https://www.youtube.com/watch?v=buR8rsf2_ls)

<https://www.youtube.com/watch?v=0H8ogvjg2TU>

<https://www.youtube.com/watch?v=jYd8kWvERj0>

#### 4. Discussion

A non-passive environment in the context of teleoperation systems refers to an environment where the forces exerted on the slave's side are not purely passive. This means that the slave's side does not simply follow the master's movements passively but may exert forces or exhibit behaviors that are independent or reactive to the master's commands. Building an experimental setup to replicate a non-passive environment presents several challenges due to its inherent complexity and unpredictability. To address these challenges, we conduct a simulation scenario in this study. Key performance indicators in a non-passive teleoperation environment include the closeness of position responses between the master and slave sides and the consistency of force tracking. Smaller errors in position and force tracking generally indicate better system performance.

##### 4.1. Case 3: Free Motion (Simulation)

Additionally, a more general free-motion case is considered, where the joint 1 of the master moves approximately up to 1 rad and then gradually returns to its original position. During the same period, joint 2 smoothly pulls out. The simulation responses are shown in Figures 12–17, and the comparisons of position errors with different control methods are summarized in Table 5. Furthermore, the related control signals regarding to P + dC, SC, and ASC are shown in Figures 13, 15 and 17, respectively. It can be observed that the proposed ASC method can provide better trajectory-tracking capability.

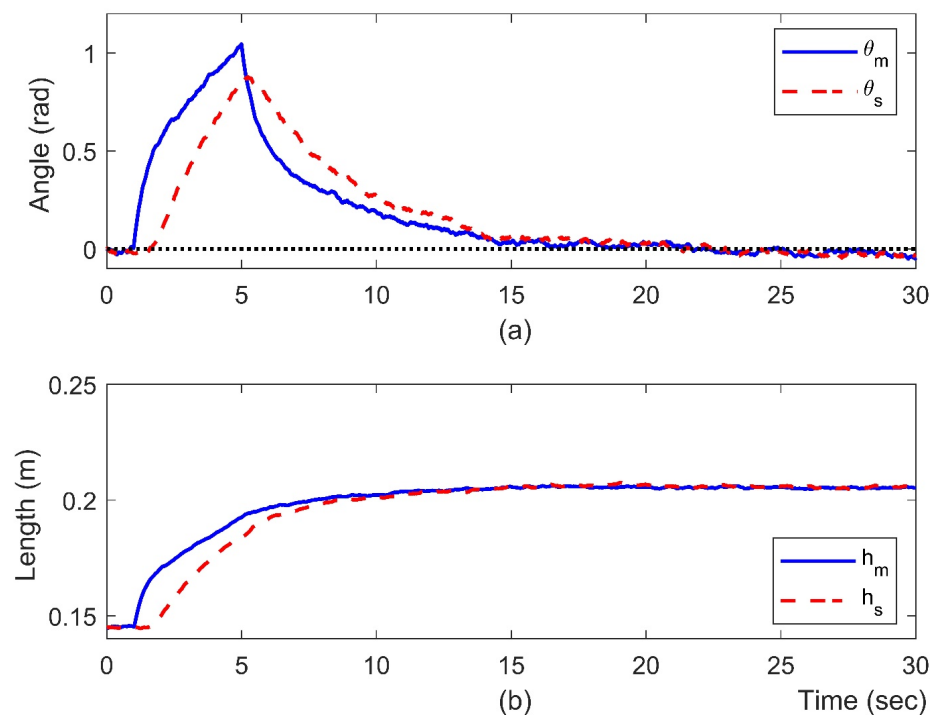


**Figure 12.** Position responses with P + dC method (Case 3): (a) joint 1, and (b) joint 2.

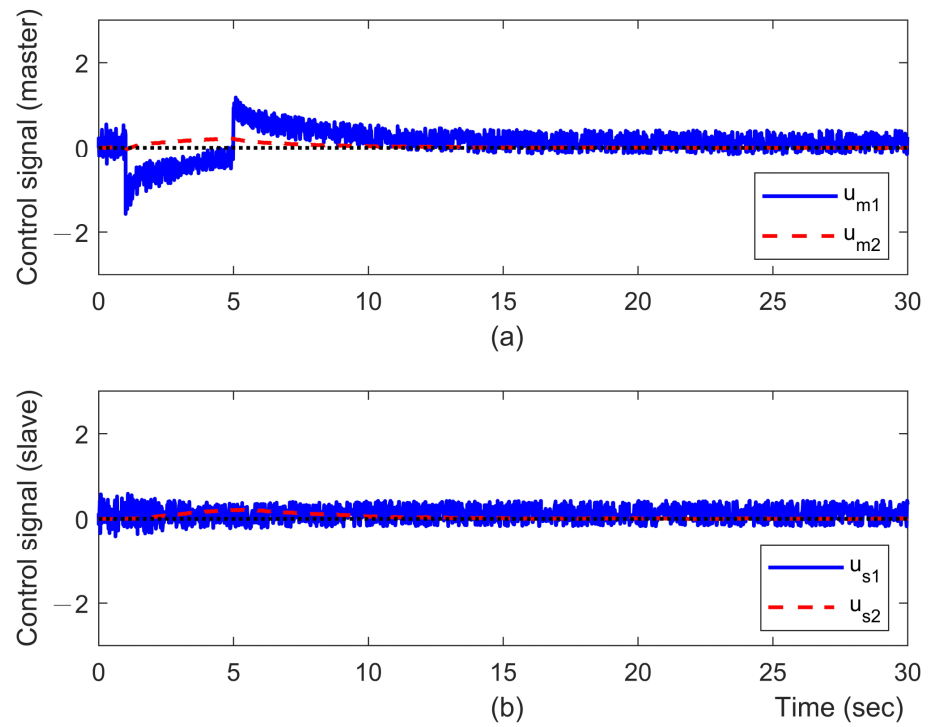


Figure 13. Control signals with P + dC method (Case 3): (a) master, and (b) slave.

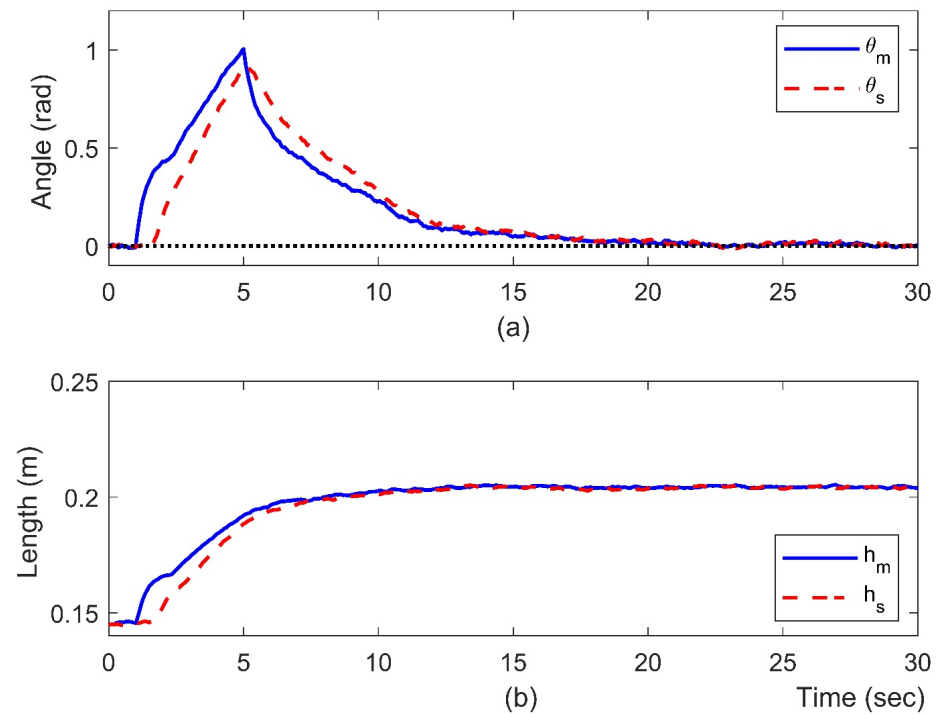


Figure 14. Position responses with SC method (Case 3): (a) joint 1, and (b) joint 2.

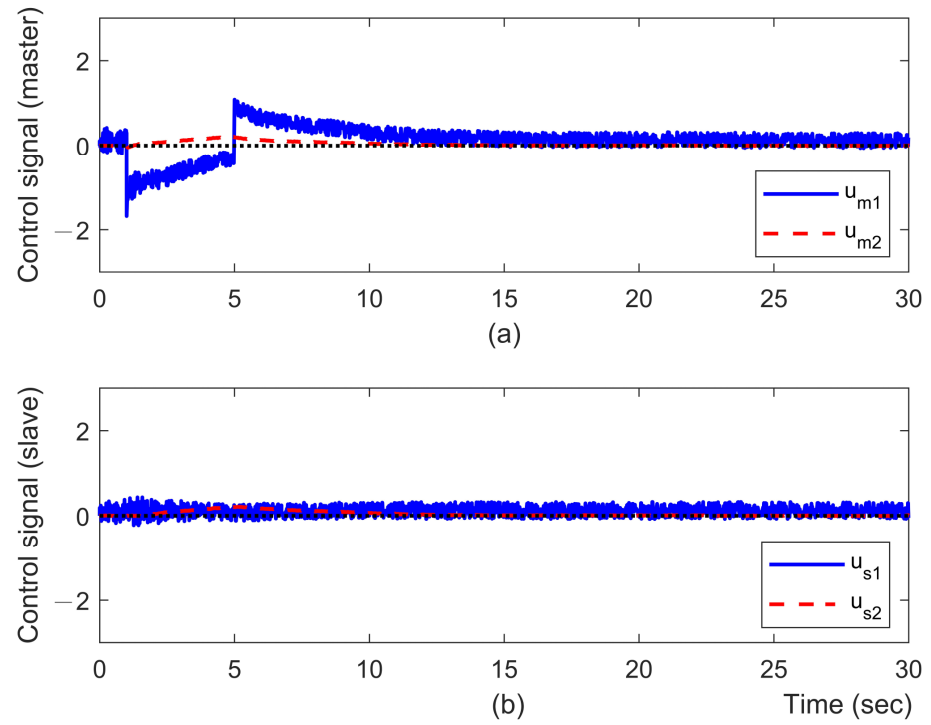


Figure 15. Control signals with SC method (Case 3): (a) master, and (b) slave.

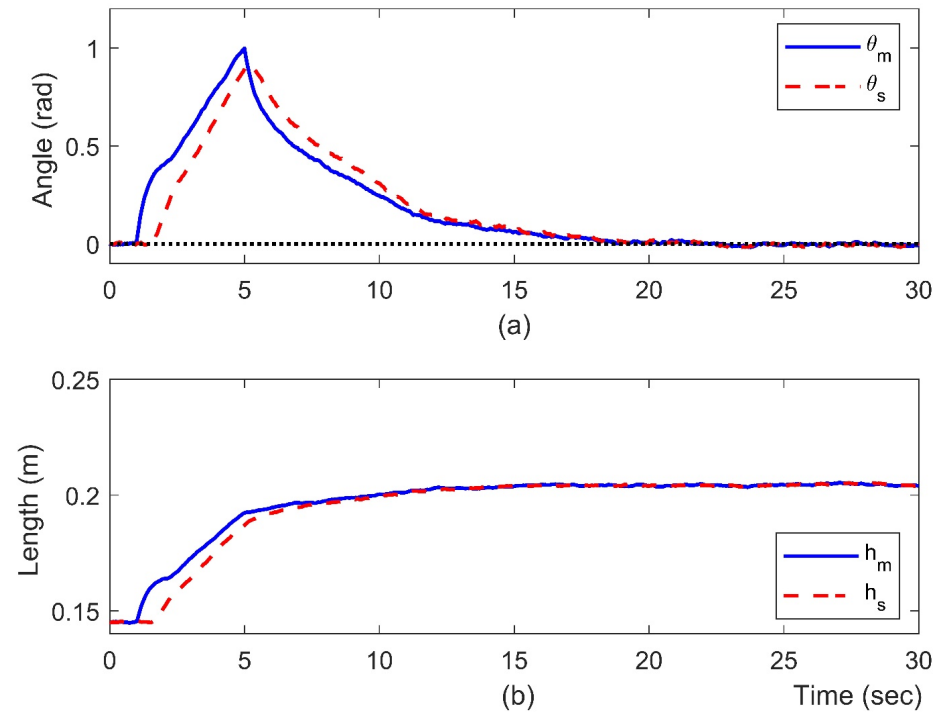


Figure 16. Position responses with ASC method (Case 3): (a) joint 1, and (b) joint 2.

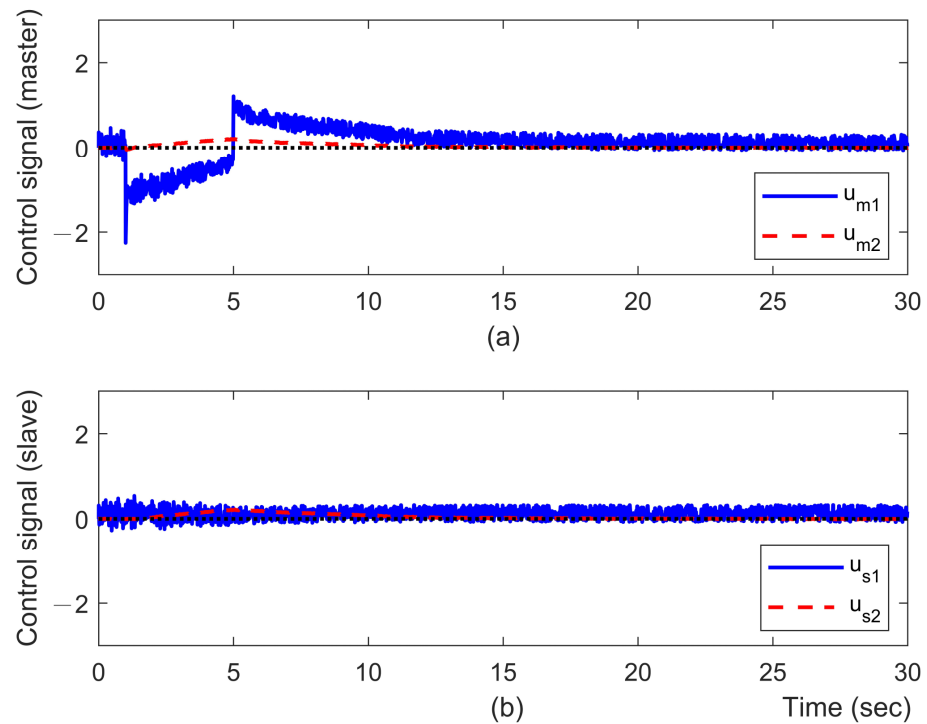


Figure 17. Control signals with ASC method (Case 3): (a) master, and (b) slave.

Table 5. Simulation comparisons of position errors in Case 3.

		IAE	ITAE	ISE	ITSE
P + dC	Joint 1	1366.5	15,168.1	179.2	1456.9
	Joint 2	26.8	296.3	0.09	0.61
SC	Joint 1	710.1	7420.9	54.4	410.4
	Joint 2	20.5	249.7	0.04	0.32
ASC	Joint 1	643.1	7295.7	44.5	369.0
	Joint 2	18.7	209.6	0.03	0.29

unit: joint 1 (rad), joint 2 (m).

#### 4.2. Case 4: Non-Passive Human and Environment (Simulation)

Consider the case that the human operator and environment forces are all non-passive, such as

$$f_h = \begin{cases} k_h - D_h \dot{q}_m - K_h q_m, & 1 \leq t \leq 30 \text{ s} \\ 0 & \text{otherwise} \end{cases} \quad (40)$$

$$f_e = \begin{cases} k_e - D_e \dot{q}_s - K_e q_s, & 5 \leq t \leq 30 \text{ s} \\ 0 & \text{otherwise} \end{cases} \quad (41)$$

where  $k_h = [-0.9 \ 0.2]^T$ ,  $k_e = [0.1 \ -0.15]^T$ ,  $D_h = D_e = \text{diag}\{1, 1\}$ , and  $K_h = K_e = \text{diag}\{1, 1\}$ .

The simulation results of this case are depicted in Figures 18–26, including the position responses, force responses, and control signals of the master and slave robots. The observation revolves around the responses after the addition of the environment force, i.e., from 5 to 30 s. From Figure 24, compared to Figures 18 and 21, the position errors of the master and slave robots are significantly improved using the proposed ASC method. As regards the force responses shown in Figures 19, 22 and 25, all three methods can support a

certain degree of inconsistency in the human and environment forces. Similarly, the average position and force errors of 20 repetitions are summarized, from 5 to 30 s, in Tables 6 and 7. It can be observed that the proposed ASC scheme has better performance in both position following and force perception.

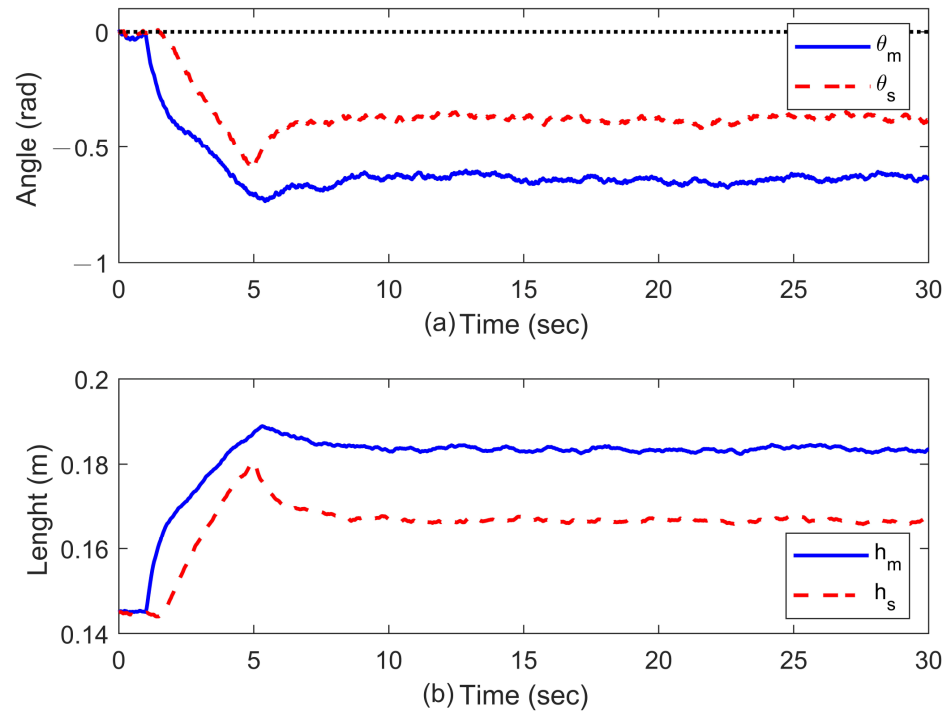


Figure 18. Position responses with P + dC method (Case 4): (a) joint 1, and (b) joint 2.

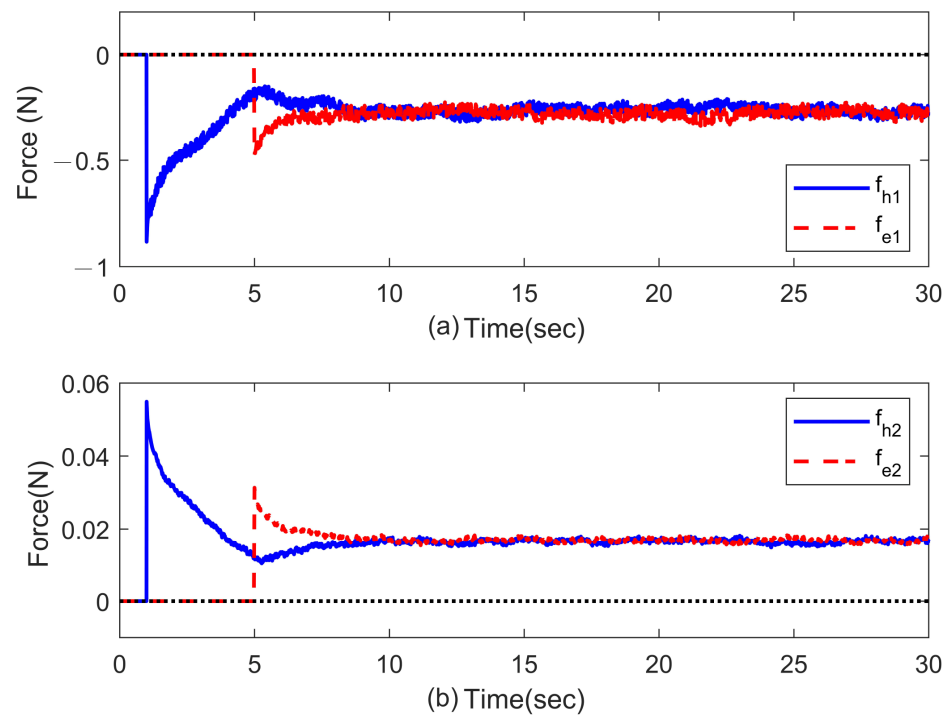


Figure 19. Force responses with P + dC method (Case 4): (a) joint 1, and (b) joint 2.

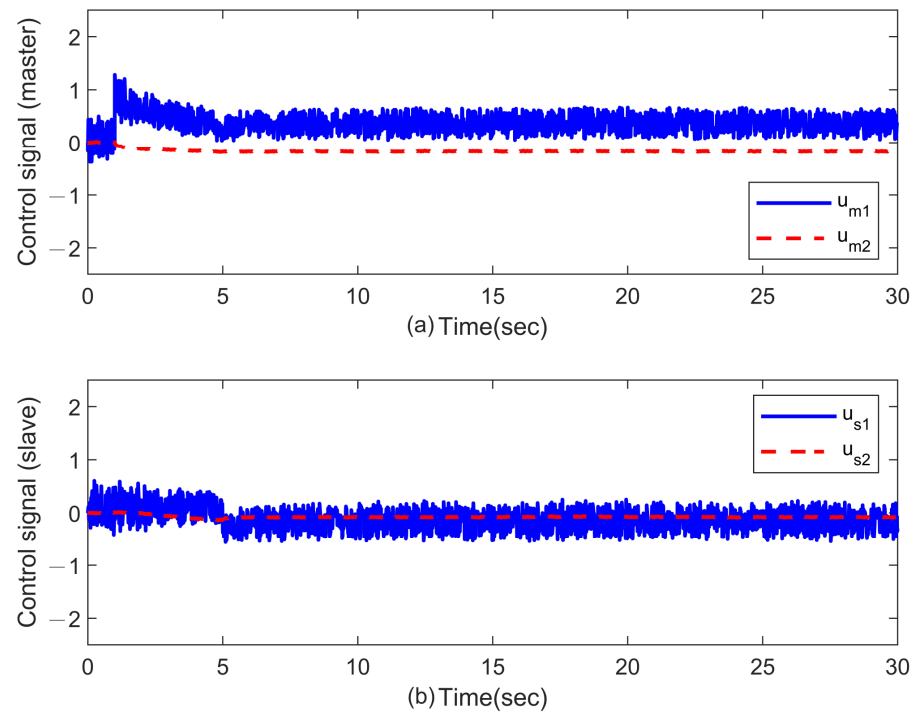


Figure 20. Control signals with P + dC method (Case 4): (a) master, and (b) slave.

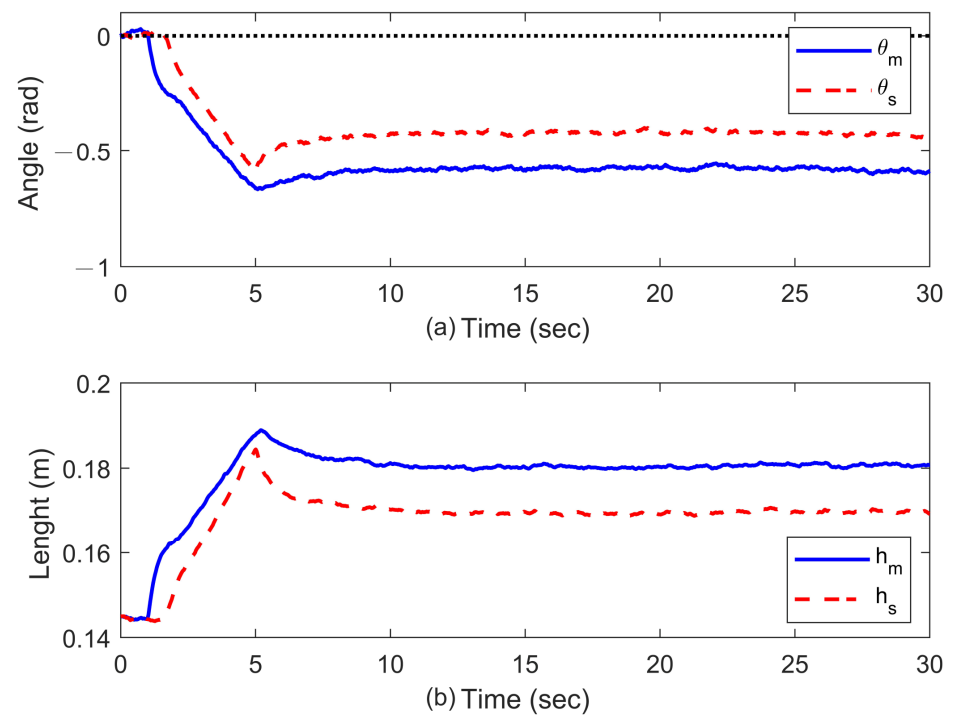


Figure 21. Position responses with SC method (Case 4): (a) joint 1, and (b) joint 2.

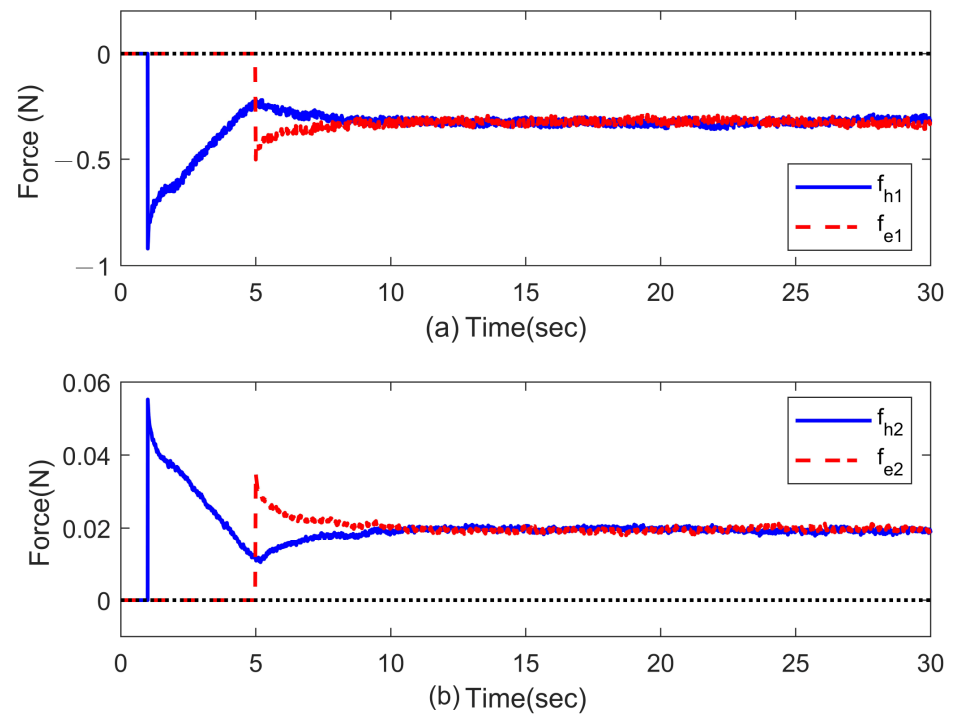


Figure 22. Force responses with SC method (Case 4): (a) joint 1, and (b) joint 2.

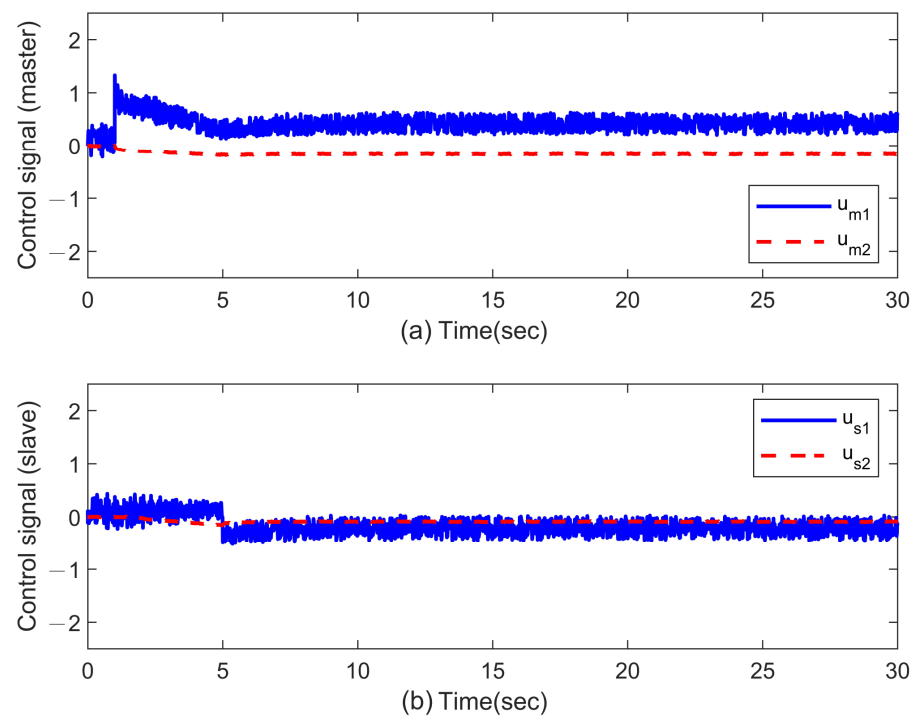


Figure 23. Control signals with SC method (Case 4): (a) master, and (b) slave.

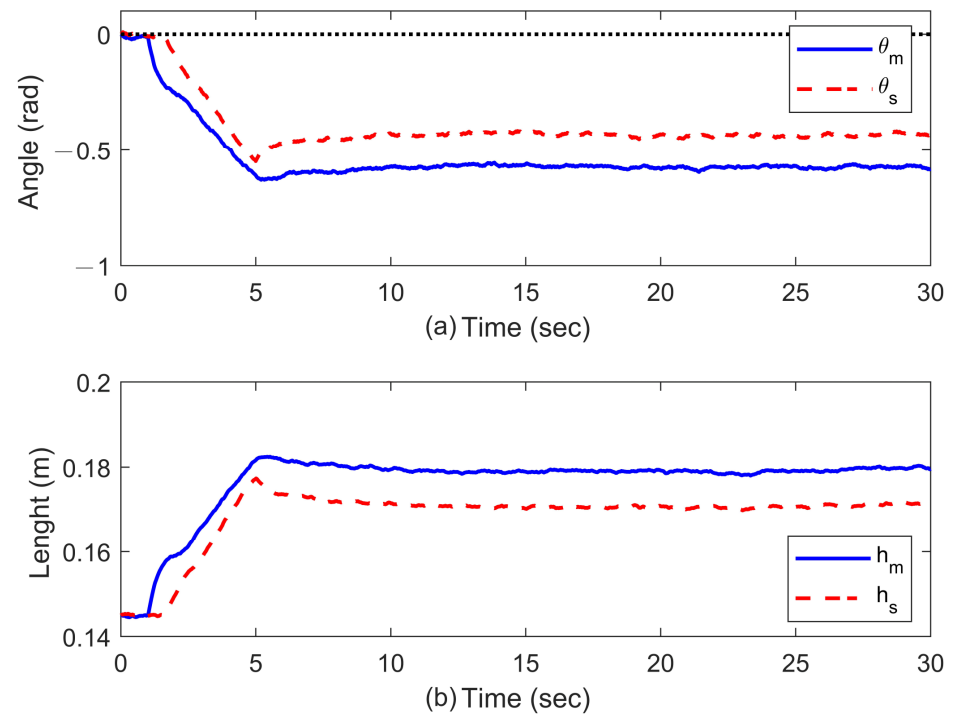


Figure 24. Position responses with ASC method (Case 4): (a) joint 1, and (b) joint 2.

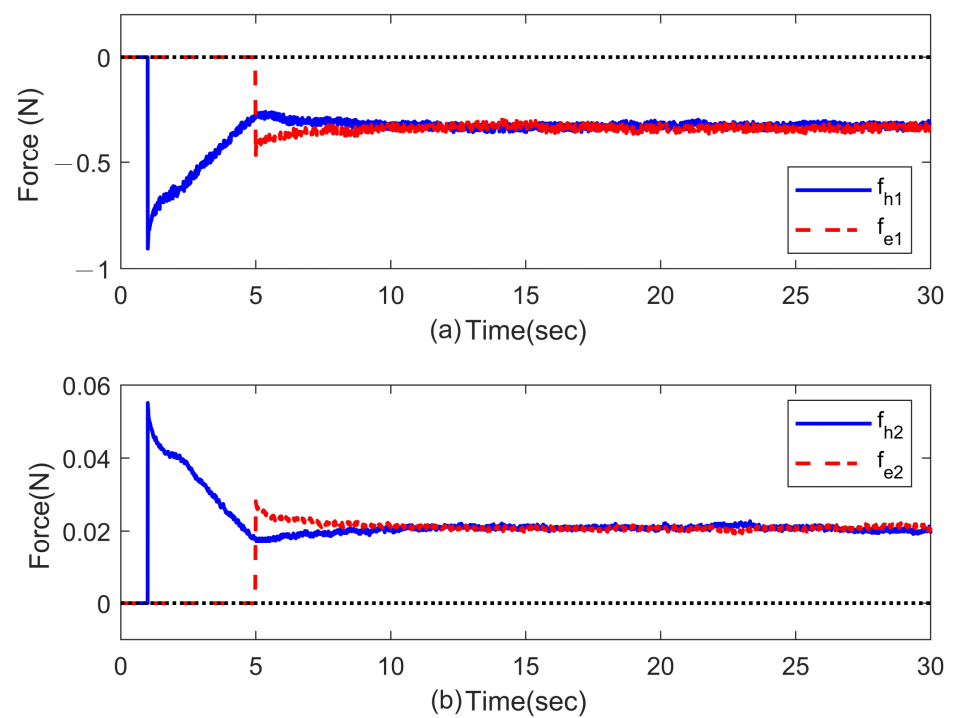


Figure 25. Force responses with ASC method (Case 4): (a) joint 1, and (b) joint 2.

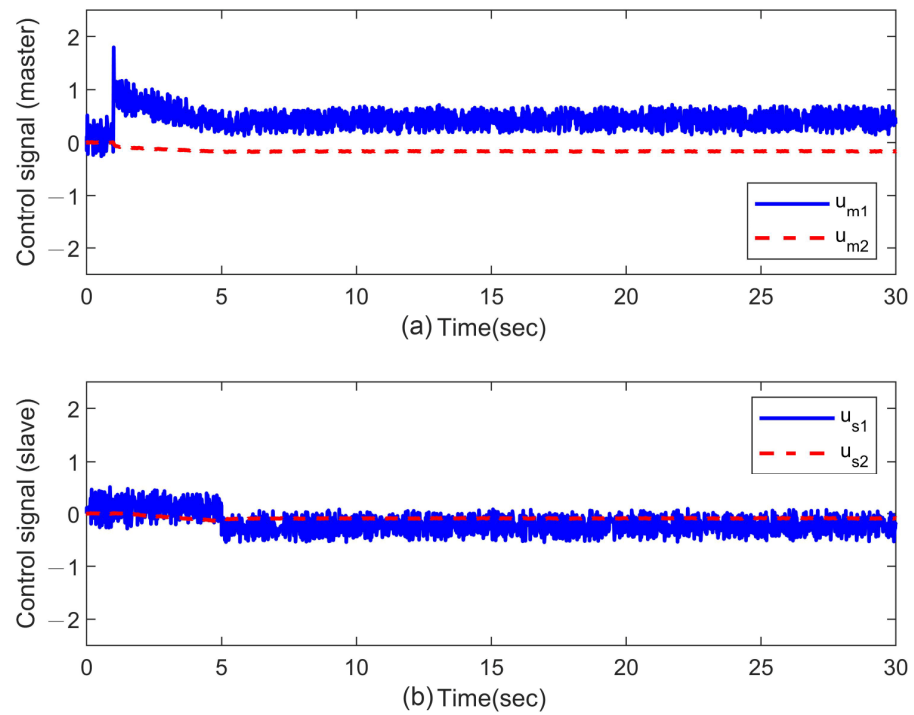


Figure 26. Control signals with ASC method (Case 4): (a) master, and (b) slave.

Table 6. Simulation comparisons of position errors in Case 4.

		IAE	ITAE	ISE	ITSE
P + dC	Joint 1	66,092.74	116,329.60	1753.97	30,999.84
	Joint 2	413.14	7264.24	6.85	120.94
SC	Joint 1	4312.21	75,538.54	747.91	13,093.91
	Joint 2	271.31	4772.02	2.95	52.16
ASC	Joint 1	3328.01	58,510.62	444.31	7840.92
	Joint 2	207.80	3637.15	1.73	30.30

unit: joint 1 (rad), joint 2 (m).

Table 7. Simulation comparisons of force errors in Case 4.

		IAE	ITAE	ISE	ITSE
P + dC	Joint 1	655.09	8101.66	49.21	355.33
	Joint 2	44.38	508.72	0.24	1.61
SC	Joint 1	643.66	7720.72	44.83	322.15
	Joint 2	35.56	353.51	0.19	1.08
ASC	Joint 1	572.32	5399.46	23.56	153.96
	Joint 2	26.39	168.89	0.08	0.19

unit: joint 1 (N), joint 2 (N).

### 5. Conclusions

This paper introduces an adaptive-sliding-mode controller that has been designed for a bilateral teleoperation system that is characterized by time-varying communication delays and unknown but bounded uncertainties. The master and slave devices utilized in the system are self-made by the authors, with certain components manufactured using CNC milling and lathe machines. The controller design involves deriving a delay-dependent

condition for stability and determining the admissible bound of time delays through linear matrix inequalities. The closed-loop stability of the teleoperation system is ensured via Lyapunov–Krasovskii stability analysis, aligning the stability analysis with the designed controllers and adaptive laws. Both passive and non-passive scenarios involving the human operator and the environment are considered in the design process. A real experimental setup is employed to validate the proposed control scheme, covering free-motion and force-perception tasks. Results indicate that the proposed adaptive-sliding-control method increases position performance from 58.48% to 82.55% and force performance from 83.48% to 99.77%. In conclusion, the proposed control algorithm shows promising potential for application in generalized haptic devices with expanded degrees of freedom. Additionally, our control strategies have successfully addressed a wide range of scenarios and environments, including free motion, force perception, and also both passive and non-passive situations. Furthermore, our experimental results underscore its viability for real-world applications.

**Author Contributions:** Conceptualization, Y.-H.C. and C.-Y.Y.; methodology, Y.-H.C., C.-Y.Y. and H.-W.L.; software, C.-Y.Y.; validation, Y.-H.C. and C.-Y.Y.; formal analysis, Y.-H.C., C.-Y.Y. and H.-W.L.; investigation, Y.-H.C. and C.-Y.Y.; data curation, C.-Y.Y.; writing—original draft preparation, Y.-H.C. and C.-Y.Y.; writing—review and editing, Y.-H.C. and H.-W.L.; visualization, Y.-H.C. and C.-Y.Y.; supervision, Y.-H.C. and H.-W.L. All authors have read and agreed to the published version of the manuscript.

**Funding:** This research received no external funding.

**Data Availability Statement:** The original contributions presented in the study are included in the article, further inquiries can be directed to the corresponding author.

**Conflicts of Interest:** The authors declare no conflicts of interest.

## References

1. Moniruzzaman, M.; Rassau, A.; Chai, D.; Islam, S. Teleoperation methods and enhancement techniques for mobile robots: A comprehensive survey. *Robot. Auton. Syst.* **2022**, *150*, 103973. [[CrossRef](#)]
2. Shahbazi, M.; Atashzar, S.F.; Patel, R.V. A systematic review of multilateral teleoperation systems. *IEEE Trans. Haptics* **2018**, *11*, 338–356. [[CrossRef](#)] [[PubMed](#)]
3. Courtois, H.; Aouf, N.; Ahiska, K.; Cecotti, M. OAST: Obstacle avoidance system for teleoperation of UAVs. *IEEE Trans. Human-Mach. Syst.* **2022**, *52*, 157–168. [[CrossRef](#)]
4. Zhang, D.; Yang, G.; Khurshid, R.P. Haptic teleoperation of UAVs through control barrier functions. *IEEE Trans. Haptics* **2020**, *13*, 109–115. [[CrossRef](#)] [[PubMed](#)]
5. Lee, M.; Lee, D. A Distributed two-layer framework for teleoperated platooning of fixed-wing UAVs via decomposition and backstepping. *IEEE Robot. Autom. Lett.* **2021**, *6*, 3655–3662. [[CrossRef](#)]
6. Fu, J.; Rota, A.; Shufei Li, A.; Zhao, J.; Liu, Q.; Iovene, E.; Ferrigno, G.; Momi, E. Recent advancements in augmented reality for robotic applications: A survey. *Actuators* **2023**, *12*, 323. [[CrossRef](#)]
7. Zhang, Q.; Liu, Q.; Duan, J.; Qin, J. Research on teleoperated virtual reality human–robot five-dimensional collaboration system. *Biomimetics* **2023**, *8*, 605. [[CrossRef](#)]
8. Song, C.; Yang, G.; Park, S.; Jang, N.; Jeon, S.; Oh, S.-R.; Hwang, D. On the design of Integrated tele-monitoring operation system for therapeutic devices in isolation intensive care unit. *IEEE Robot. Autom. Lett.* **2022**, *7*, 8705–8712. [[CrossRef](#)]
9. Aggravi, M.; Estima, D.A.L.; Krupa, A.; Misra, S.; Pacchierotti, C. Haptic teleoperation of flexible needles combining 3D ultrasound guidance and needle tip force feedback. *IEEE Robot. Autom. Lett.* **2021**, *6*, 4859–4866. [[CrossRef](#)]
10. Feng, F.; Zhou, Y.; Hong, W.; Li, K.; Xie, L. Development and experiments of a continuum robotic system for transoral laryngeal surgery. *Int. J. Comput. Assist. Radiol. Surg.* **2022**, *17*, 479–505. [[CrossRef](#)]
11. Wakasa, Y.; Hakamada, K.; Morohashi, H.; Kanno, T.; Tadano, K.; Kawashima, K.; Ebihara, Y.; Oki, E.; Hirano, S.; Mori, M. Ensuring communication redundancy and establishing a telementoring system for robotic telesurgery using multiple communication line. *J. Robot. Surg.* **2024**, *18*, 9. [[CrossRef](#)]
12. Zhaoa, B.; Nelson, C.A. A sensorless force-feedback system for robot assisted laparoscopic surgery. *Comput. Assist. Surg.* **2019**, *24*, 36–43. [[CrossRef](#)] [[PubMed](#)]
13. Schleer, P.; Körner, D.; Vossel, M.; Drobinsky, S.; Radermacher, K. Conceptual design of force reflection control for teleoperated bone surgery. *Curr. Dir. Biomed. Eng.* **2020**, *6*, 20200014. [[CrossRef](#)]

14. Muñoz, V.F.; Garcia-Morales, I.; Fraile-Marinero, J.C.; Perez-Turiel, J.; Muñoz-Garcia, A.; Bauzano, E.; Rivas-Blanco, I.; Sabater-Navarro, J.M.; de la Fuente, E. Collaborative robotic assistant platform for endonasal surgery: Preliminary in-vitro trials. *Sensors* **2021**, *21*, 2320. [[CrossRef](#)]
15. Quek, Z.F.; Provancher, W.R.; Okamura, A.M. Evaluation of skin deformation tactile feedback for teleoperated surgical tasks. *IEEE Trans. Haptics* **2019**, *12*, 102–113. [[CrossRef](#)] [[PubMed](#)]
16. Patel, R.V.; Atashzar, S.F.; Tavakoli, M. Haptic feedback and force-based teleoperation in surgical robotics. *Proc. IEEE* **2022**, *110*, 1012–1027. [[CrossRef](#)]
17. Gong, Y.; Ji, Y. A Novel Passivity Criterion for bilateral teleoperation under event triggered PD-like control with constant time delays. *Int. J. Control Autom. Syst.* **2022**, *20*, 2353–2363. [[CrossRef](#)]
18. Bao, J.; Fu, L.; Zhang, H.; Zhang, A.; Guo, W.; Chen, T. An adaptive proportional plus damping control for teleoperation systems with asymmetric time-varying communication delays. *Mathematics* **2022**, *10*, 4675. [[CrossRef](#)]
19. Ahmad, U.; Pan, Y.-J. A Time Domain Passivity approach for asymmetric multilateral teleoperation system. *IEEE Access* **2018**, *6*, 519–531. [[CrossRef](#)]
20. Ryu, J.-H.; Ha-Van, Q.; Jafari, A. Multilateral teleoperation over communication time delay using the time-domain passivity approach. *IEEE Trans. Control Syst. Technol.* **2020**, *28*, 2705–2712. [[CrossRef](#)]
21. Bavili, R.E.; Akbari, A.; Esfanjani, R.M. Passivity-based control of nonlinear teleoperation systems with non-passive interaction forces. *Intell. Serv. Robot.* **2020**, *13*, 419–437. [[CrossRef](#)]
22. Li, W.; Liu, Y.; Ding, L.; Wang, J.; Gao, H.; Deng, Z. Teleoperation of wheeled mobile robots subject to longitudinal slipping and lateral sliding by time-domain passivity controller. *Mechatronics* **2022**, *81*, 102705. [[CrossRef](#)]
23. Gong, X.; Wang, L.; Mou, Y.; Wang, H.; Wei, X.; Zheng, W.; Yin, L. Improved four-channel PBTDPA control strategy using force feedback bilateral teleoperation system. *Int. J. Control Autom. Syst.* **2022**, *20*, 1002–1017. [[CrossRef](#)]
24. Li, R.; Cheng, M.; Ding, R. Passivity-based bilateral shared variable impedance control for teleoperation compliant assembly. *Mechatronics* **2023**, *95*, 10305. [[CrossRef](#)]
25. Uyulan, C. Robust passivity-based nonlinear controller design for bilateral teleoperation system under variable time delay and variable load disturbance. *Nonlinear Eng.* **2024**, *13*, 20220358. [[CrossRef](#)]
26. Sun, D.; Naghdy, F.; Du, H. Neural Network-based Passivity Control of Teleoperation System under Time-Varying Delays. *IEEE Trans. Cybern.* **2017**, *47*, 1666–1680. [[CrossRef](#)] [[PubMed](#)]
27. Yang, L.; Chen, Y.; Liu, Z.; Chen, K.; Zhang, Z. Adaptive Fuzzy Control for Teleoperation System with Uncertain Kinematics and Dynamics. *Int. J. Control Autom. Syst.* **2019**, *17*, 1158–1166. [[CrossRef](#)]
28. Li, H.; Chou, W. Adaptive FNN backstepping control for nonlinear bilateral teleoperation with asymmetric time delays and uncertainties. *Int. J. Control Autom. Syst.* **2023**, *21*, 3091–3104. [[CrossRef](#)]
29. Su, S.; Ji, Y. Fixed-time adaptive neural network synchronization control for teleoperation system with position error constraints and time-varying delay. *Nonlinear Dyn.* **2023**, *111*, 13053–13072. [[CrossRef](#)]
30. Kebria, P.M.; Khosravi, A.; Nahavandi, S.; Wu, D.; Bello, F. Adaptive type-2 fuzzy neural-network control for teleoperation systems with delay and uncertainties. *IEEE Trans. Fuzzy Syst.* **2020**, *28*, 2543–2554. [[CrossRef](#)]
31. Sun, D.; Liao, Q.; Stoyanov, T.; Kiselev, A.; Loutfi, A. Bilateral telerobotic system using type-2 fuzzy neural network based moving horizon estimation force observer for enhancement of environmental force compliance and human perception. *Automatica* **2019**, *106*, 358–373. [[CrossRef](#)]
32. Zhang, J.; Xia, M.; Li, S.; Liu, Z.; Yang, J. The adaptive bilateral control of underwater manipulator teleoperation system with uncertain parameters and external disturbance. *Electronics* **2024**, *13*, 1122. [[CrossRef](#)]
33. Huang, F.; Zhang, W.; Chen, Z.; Tang, J.; Song, W.; Zhu, S. RBFNN-based adaptive sliding mode control design for nonlinear bilateral teleoperation system under time-varying delays. *IEEE Access* **2019**, *7*, 11905–11912. [[CrossRef](#)]
34. Hao, S.; Hu, L.; Liu, P.X. Sliding mode control for a surgical teleoperation system via a disturbance observer. *IEEE Access* **2019**, *7*, 43383. [[CrossRef](#)]
35. Hu, J.; Zhang, H.; Liu, H.; Yu, X. A survey on sliding mode control for networked control systems. *Int. J. Syst. Sci.* **2021**, *52*, 1129–1147. [[CrossRef](#)]
36. Guajardo-Benavides, E.; Arteaga, M. On the finite time force estimation for bilateral teleoperation of robot manipulators with time varying delays. *Control Eng. Pract.* **2023**, *138*, 105622. [[CrossRef](#)]
37. Zhang, H.; Song, A.; Li, H.; Chen, D.; Fan, L. Adaptive finite-time control scheme for teleoperation with time-varying delay and uncertainties. *IEEE Trans. Syst. Man Cybern. Syst.* **2022**, *52*, 1552–1566. [[CrossRef](#)]
38. Guo, S.; Liu, Z.; Li, L.; Ma, Z.; Huang, P. Fixed-time personalized variable gain tracking control for teleoperation systems with time varying delays. *J. Frankl. Inst.* **2023**, *360*, 13015–13032. [[CrossRef](#)]
39. Dehghan, S.A.M.; Koofigar, H.R.; Sadeghian, H.; Ekramian, M. Observer-based adaptive force–position control for nonlinear bilateral teleoperation with time delay. *Control Eng. Pract.* **2021**, *107*, 104679. [[CrossRef](#)]
40. Wang, Y.; Tian, J.; Liu, Y.; Yang, B.; Liu, S.; Yin, L.; Zheng, W. Adaptive neural network control of time delay teleoperation system based on model approximation. *Sensors* **2021**, *21*, 7443. [[CrossRef](#)]
41. Tumerdem, U.; Yilmaz, N. A unifying framework for transparency optimized controller design in multilateral teleoperation with time delays. *Control Eng. Pract.* **2021**, *117*, 104931. [[CrossRef](#)]

42. Zhai, D.-H.; Xia, Y. A novel switching-based control framework for improved task performance in teleoperation system with asymmetric timevarying delays. *IEEE Trans. Cybern.* **2018**, *48*, 625–638. [[CrossRef](#)] [[PubMed](#)]
43. Nguyen, T.-V.; Liu, Y.-C. Advanced finite-time control for bilateral teleoperators with delays and uncertainties. *IEEE Access* **2021**, *9*, 141951. [[CrossRef](#)]
44. Zakerimanesh, A.; Hashemzadeh, F.; Torabi, A.; Tavakoli, M. Controlled synchronization of nonlinear teleoperation in task-space with timevarying delays. *Int. J. Control Autom. Syst.* **2019**, *17*, 1875–1883. [[CrossRef](#)]
45. Hua, C.-C.; Liu, X.P. Delay-dependent stability criteria of teleoperation systems with asymmetric time-varying delays. *IEEE Trans. Robot.* **2010**, *26*, 925–932. [[CrossRef](#)]
46. Deepak, V.; Arun, N.K.; Shihabudheen, K.V. Observer based stabilization of linear time delay systems using new augmented LKF. *IFAC J. Syst. Control* **2023**, *26*, 100231. [[CrossRef](#)]
47. Halder, K.; Gillam, L.; Dixit, S.; Mouzakitis, A.; Fallah, S. Stability analysis with LMI based distributed  $H_\infty$  controller for vehicle platooning under random multiple packet drops. *IEEE Trans. Intell. Transp. Syst.* **2022**, *23*, 23517–23532. [[CrossRef](#)]
48. Yang, Y.; Constantinescu, D.; Shi, Y. Input-to-state stable bilateral teleoperation by dynamic interconnection and damping injection: Theory and experiments. *IEEE Trans. Ind. Electron.* **2020**, *67*, 790–799. [[CrossRef](#)]
49. Baranitha, R.; Rakkiyappan, R.; Li, X. T-S fuzzy model-based singlemaster multislave teleoperation systems with decentralized communication structure and varying time delays. *IEEE Trans. Fuzzy Syst.* **2020**, *28*, 3406–3417. [[CrossRef](#)]
50. Bavili, R.E.; Akbari, A.; Esfanjani, R.M. Controller design for nonlinear bilateral teleoperation systems via total energy shaping. *Mech. Syst. Signal Process.* **2021**, *150*, 107239. [[CrossRef](#)]
51. Estrada, E.; Yu, W.; Li, X. Stable bilateral teleoperation with phase transition and haptic feedback. *J. Frankl. Inst.* **2021**, *358*, 1940–1956. [[CrossRef](#)]
52. Islam, S.; Liu, X.P.; Saddik, A. Nonlinear adaptive control for teleoperation systems with symmetrical and unsymmetrical time-varying delay. *Int. J. Syst. Sci.* **2015**, *46*, 2928–2938. [[CrossRef](#)]
53. Islam, S.; Liu, P.X.; Saddik, A.E. Nonlinear control for teleoperation systems with time varying delay. *Nonlinear Dyn.* **2014**, *76*, 931–954. [[CrossRef](#)]
54. Islam, A.; Liu, P.X.; Saddik, A.E.; Yang, Y.B. Bilateral control of teleoperation systems with time delay. *IEEE/ASME Trans. Mechatronics* **2015**, *20*, 1–12. [[CrossRef](#)]
55. Hu, J.; Wang, Z.; Gao, H.; Stergioulas, L.K. Robust sliding mode control for discrete stochastic systems with mixed time delays randomly occurring uncertainties, and randomly occurring nonlinearities. *IEEE Trans. Ind. Electron.* **2012**, *59*, 3008–3015. [[CrossRef](#)]
56. Sun, Y.G.; Wang, L.; Xie, G. Average consensus in networks of dynamic agents with switching topologies and multiple time-varying delays. *Syst. Control Lett.* **2008**, *57*, 175–183. [[CrossRef](#)]
57. Chang, Y.-H.; Chan, W.-S. Adaptive dynamic surface control for uncertain nonlinear systems with interval type-2 fuzzy neural networks. *IEEE Trans. Cybern.* **2014**, *44*, 293–304. [[CrossRef](#)]

**Disclaimer/Publisher’s Note:** The statements, opinions and data contained in all publications are solely those of the individual author(s) and contributor(s) and not of MDPI and/or the editor(s). MDPI and/or the editor(s) disclaim responsibility for any injury to people or property resulting from any ideas, methods, instructions or products referred to in the content.